Mechanosensitive mTORC2 independently coordinates leading and trailing edge polarity programs during neutrophil migration

Suvrajit Saha[1], Jason P. Town[1], and Orion D. Weiner[1*]

[1] Cardiovascular Research Institute and Department of Biochemistry and Biophysics, University of California, San Francisco, California, United States of America

* Address correspondence to: Orion D. Weiner (orion.weiner@ucsf.edu)

Running title: mTORC2 coordinates front-back polarity

Abbreviations used: dHL-60, differentiated HL-60 cell; fMLP, N-Formylmethionine-leucyl-phenylalanine; F-actin, filamentous actin; mTOR, mechanistic target of rapamycin; mTORC2, mTOR complex 2; PIP_3, Phosphatidylinositol (3,4,5)-trisphosphate; PI3K, phosphoinositide 3-kinase; pPAK, phosphorylated p21-activated kinase; pMLC, phosphorylated myosin regulatory light chain; Rac, Ras-related C3 botulinum toxin substrate; shRNA, small hairpin RNA

ABSTRACT

By acting both upstream and downstream of biochemical organizers of the cytoskeleton, physical forces function as central integrators of cell shape and movement. Here we use a combination of genetic, pharmacological, and optogenetic perturbations to probe the role of the conserved mechanosensitive mTORC2 programs in neutrophil polarity and motility. We find that the tension-based inhibition of leading edge signals (Rac, F-actin) that underlies protrusion competition is gated by the kinase-independent role of the complex, whereas the regulation of RhoA and Myosin II-based contractility at the trailing edge depend on mTORC2 kinase activity. mTORC2 is essential for spatial and temporal coordination of the front and back polarity programs for persistent migration under confinement. This mechanosensory pathway integrates multiple upstream signals, and we find that membrane stretch synergizes with biochemical co-input PIP_3 to robustly amplify mTORC2 activation. Our results suggest that different signalling arms of mTORC2 regulate spatially and molecularly divergent cytoskeletal programs for efficient coordination of neutrophil shape and movement.

INTRODUCTION

Directed cell migration underlies a wide range of physiological processes ranging from developmental morphogenesis to immune cell responses (SenGupta *et al.*, 2021). Single cells move by extending a leading front that protrudes and a trailing rear that contracts and follows the front. These programs exhibit not only spatial compartmentalization of distinct intracellular signals to either the front or back of the cell (polarization) but also temporal coordination between these domains (Xu *et al.*, 2003). Neutrophils are a type of innate immune cell that rely on properly oriented cell polarity to migrate to sites of injury where they hunt and kill invading pathogens (Lämmermann *et al.*, 2013). In the cell front, activation of small GTPase Rac helps sets the permissive zone for WAVE-regulatory complex (WRC)-dependent actin polymerisation in protrusions (Weiner *et al.*, 2007; Koronakis *et al.*, 2011). At the back, the GTPase RhoA stimulates myosin based contractility (Wong *et al.*, 2006; Hind *et al.*, 2016; Tsai *et al.*, 2019). These signaling domains are sustained by short-range positive feedback loops within the modules and are spatially separated by mutual antagonism between them (Xu *et al.*, 2003; Ku *et al.*, 2012). Coordination within and between the modules is critical for polarity maintenance during persistent migration (Tsai *et al.*, 2019), but how this coordination is achieved is not fully understood.

When cells protrude or contract, they alter the mechanical properties of the cell surface. While mechanics was initially seen as a downstream output of cytoskeletal dynamics, emerging evidence suggest that mechanics feeds back to regulate the upstream leading and trailing edge biochemical signals (Diz-Muñoz *et al.*, 2013; Mueller *et al.*, 2017; Saha *et al.*, 2018; Hetmanski *et al.*, 2019). In neutrophils, membrane tension acts as a long-range inhibitor of actin nucleation and polymerization to constrain the size and number of cell protrusions

(Houk *et al.*, 2012). Increases in membrane tension triggers a mechanosensitive signalling cascade to regulate actin dynamics in neutrophils. Actin-based polymerization in protrusions stimulates Mechanistic target of Rapamycin Complex 2 (mTORC2) through the activation of Phospholipase D2. By connecting increases in protrusion to decreases in actin nucleation, mTORC2 is a central component of the negative-feedback-based homeostat on membrane tension (Diz-Muñoz *et al.*, 2016).

mTOR kinase is an ancient and evolutionarily conserved regulator of cell growth, proliferation, and survival (Saxton and Sabatini, 2017). mTOR forms two distinct multi-subunit complexes in mammalian cells mTOR complex 1 (mTORC1) and mTOR complex 2 (mTORC2). mTORC2 is formed from the association of core mTOR subunits with Rictor and mSin1. Rictor scaffolds the complex and is indispensable for the stability of the complex, whereas mSin1 aids the kinase activity of the complex (Jacinto *et al.*, 2004; Sarbassov *et al.*, 2004; Frias *et al.*, 2006). TORC2 activity is thought to broadly localize to plasma membrane (Ebner *et al.*, 2017b; Riggi *et al.*, 2020), where it relays growth factor signals by phosphorylating its downstream effectors Akt, PKC and SGK1 and other targets to regulate a wide range of cellular processes including cytoskeletal organisation and cell migration (Saxton and Sabatini, 2017).

mTORC2 plays a homeostatic role in response to membrane stretch in a wide variety of cell types, ranging from yeast (Berchtold *et al.*, 2012; Riggi *et al.*, 2018) to immune cells (Diz-Muñoz *et al.*, 2016) to *Dictyostelium* (Kamimura *et al.*, 2008). In *S. cerevisiae*, plasma membrane (PM) stretch activates TORC2 to stimulate sphingolipid biosynthesis, sterol recycling and bilayer asymmetry as homeostatic mechanisms to reset membrane tension and restore membrane trafficking (Riggi *et al.*, 2020). In neutrophils, where membrane tension

increases arise from protrusive forces of F-actin, mTORC2 based inhibition of actin polymerisation serves a mechanism to maintain the tension setpoint as well as restrict polarity signals (Diz-Muñoz *et al.*, 2016). A conserved role of mTORC2 also involves gating chemoattractant signaling to cyclic-AMP production to regulate myosin contractility and drive tail retraction in neutrophils (Liu *et al.*, 2010, 2014). Perturbation of mTORC2 component Rictor led to impaired chemotaxis in neutrophils, fibroblasts and *Dictyostelium* consistent with its role in regulating actin cytoskeleton (Lee *et al.*, 2005; Liu *et al.*, 2010; Agarwal *et al.*, 2013; He *et al.*, 2013). These wide arrays of cytoskeletal defects are thought to rise from both positive (He *et al.*, 2013) and negative inputs (Diz-Muñoz *et al.*, 2016; Huang *et al.*, 2017) to front and back polarity programs and have been difficult to decouple.

Here, we investigate the logic of Rictor/mTORC2 based regulation of front and back polarity programs (**Figure 1A**). The kinase-independent roles of mTORC2 restricts actin polymerization at the cell front, whereas its kinase activity is essential for myosin contractility at the cell rear. While front/back regulation is normally highly coordinated, they lose their coordination in the absence of mTORC2. These defects are particularly profound when neutrophils explore and move in confined environments. Furthermore, membrane stretch synergizes with biochemical co-input of PIP_3 to robustly amplify mTORC2 signaling activity. Our work reveals a role for mTORC2 in coordinating front and back polarity through different effector arms of this highly-conserved mechanosensor.

RESULTS

Rictor/mTORC2 is a regulator of neutrophil ameboid motility

How is the mechanoresponsive triggering of mTORC2 linked to cell migration? One possible route to regulating motility is through altering the dynamics of actin polymerisation or myosin contractility (**Figure 1A**). Earlier studies in neutrophils using partial knockdown of Rictor or mSin1 (using shRNAs) have found both positive and negative roles of mTORC2 on cytoskeletal effectors (Rac, Cdc42, RhoA), confounding a clear understanding of the logic of this regulation (Liu *et al.*, 2010; He *et al.*, 2013; Diz-Muñoz *et al.*, 2016). We reasoned that genetic nulls with complete loss of mTORC2 specific subunits in neutrophil-like dHL-60 cells would offer a more surgical approach to dissect these mechanisms, following the success of this strategy in other cell-based models (Guertin *et al.*, 2006; Agarwal *et al.*, 2013; Huang *et al.*, 2017).

To distinguish between the relative contribution of the kinase roles of mTORC2 and the kinase-independent scaffolding roles of Rictor, we devised a CRISPR-Cas9 based approach (**Figures S1 A, B**) to knock-out two key components of mTORC2 in dHL-60 cells - its scaffolding sub-unit Rictor and its kinase accessory subunit mSin1 (**Figures 1B, C**). Rictor null (Rictor KO) cells impair both mTORC2 kinase and non-kinase roles, whereas mSin1 null (mSin1 KO) cells specifically affect the kinase roles (Jacinto *et al.*, 2004, 2006; Sarbassov *et al.*, 2004; Guertin *et al.*, 2006). As a pharmacological approach to impair the kinase function of mTOR, we used a specific inhibitor of mTOR Kinase KU-0063794 (KU) (García-Martínez *et al.*, 2009). To read out the kinase activity of mTORC2, we assayed the phosphorylation of the well-characterized mTORC2 substrate Akt (Ebner *et al.*, 2017b). When stimulated by

chemoattractant peptide formyl-Met-Leu-Phe (fMLP); neutrophil-like differentiated HL-60 (dHL-60) cells derived from both Rictor KO and mSin1KO lines show marked reduction in the phosphorylation of Akt to levels that were comparable to pharmacological inhibition of the mTOR kinase (~75-80% reduction from wildtype cells; **Figure S1C, D**), indicating a loss of mTORC2 kinase activity with all of these perturbations.

To determine the importance of these mTORC2 perturbations on cell movement, we performed a transwell chemotaxis assay (**Figure 1D**), which demonstrated that the perturbations of mTORC2 complex formation (in Rictor KO) or kinase activity (in Rictor KO, mSin1KO or mTOR kinase inhibition) all led to significant and comparable defects in bulk transwell migration (**Figure 1D**; 60-70% drop in migration index compared to WT). These results agree with earlier reports of chemotaxis defects in Rictor shRNA knockdowns and upon long term perturbation of mTOR activity with Rapamycin (Liu *et al.*, 2010; He *et al.*, 2013; Diz-Muñoz *et al.*, 2016). In addition, we find that both acute (with drug KU) and chronic perturbation (mSin1 KO) of mTOR kinase also impair transwell migration. This is consistent with chemotaxis defects observed in genetic knockouts of Rip3 (Sin1 ortholog of mSin1) in *Dictyostelium* (Lee *et al.*, 2005) but is in contrast with an earlier study using partial knockdown of mSin1 in neutrophils, which found no discernible defects in chemotactic movement of mSin1 KD cells in a micro-needle assay (He *et al.*, 2013). Factors like differences in the extent of depletion and the type of migration assay conditions used can often lead to confounding results, so we chose to assess motility defects in cleaner single cell assays of cell migration with the genetic nulls of mTORC2 components.

We suspected that mTORC2-based mechanoadaptation might be particularly important when cells are in migration environments that mechanically perturb them, including squeezing

through a pore for transwell assays or migrating under mild confinement. To study 2D migration under mild confinement, we made use of under-agarose (2% w/v) overlay on cells (Bell *et al.*, 2018; Tsai *et al.*, 2019; Brunetti *et al.*, 2022) and tracked individual cells over the course of 20-30 minutes (assay schematic and cell tracks in **Figure 1E**) in presence of uniform chemoattractant (25 nM fMLP). Both Rictor KO and mSin1 KO cells exhibited less net displacement (**Figure 1E and S2E**) and moved at significantly slower speeds (**Figure 1F**; median speed for Rictor KO: 3.2 μm/min; mSin1 KO: 6 μm/min) compared to wildtype (WT) dHL-60 cells (median speed: 9 μm/min). However, under similar assay environment, only Rictor KO cells showed a significantly reduced persistence (ratio of displacement/distance; median persistence for Rictor KO: 0.1; WT: 0.5), suggesting a role for Rictor beyond the kinase activity of mTORC2. In contrast to the defects observed under agarose, when Rictor KO and mSin1 KO cells were assayed for classical unconfined 2D-motility (**Figure S2A**) on glass coverslips coated with fibronectin, they moved with similar displacement, speed, and persistence as WT dHL-60 cells (**Figure S2 B-D**). These results suggest that migratory defects upon mTORC2 perturbation are sensitised in an assay where cells need to actively assess the local environment and adapt during movement. These results also indicate that kinase activity of mTORC2 is specifically required to set the speed of movement, while the scaffolding roles of the complex contribute to maintain persistence of motion (**Figure 1H**).

Kinase-independent roles of Rictor/mTORC2 restricts the zone of F-actin assembly to the cell front

Persistent motility in neutrophils relies on establishing a single front of lamellipodial F-actin. Earlier studies have shown that fMLP stimulated neutrophils with reduced levels of Rictor (via

shRNA knockdowns) show elevated steady-state levels of F-actin (Diz-Muñoz *et al.*, 2016) with a near-uniform peripheral distribution of actin polymerization (Liu *et al.*, 2010). While this is consistent with Rictor/mTORC2 mediating negative feedback to inhibit F-actin polymerisation (**Figure S1E**), the relative contributions of mTORC2 kinase activity and kinase-independent roles in this process remains unclear (**Figure 2A**). Answering these questions necessitates the larger suite of mTORC2 perturbations that we leverage in the current work.

To assay actin assembly in our mutant backgrounds, we stimulated fibronectin-adhered wildtype (WT), Rictor KO and mSin1 KO dHL-60 neutrophils with chemoattractant for 5 minutes to allow cells to polarize and then fixed and stained them with Phalloidin-Alexa647. Consistent with our earlier results (Diz-Muñoz *et al.*, 2016) from partial loss of Rictor (via shRNA knockdowns), Rictor KO cells exhibit significant increase in F-actin levels in polarized cells (**Figure S1E**). In contrast, depletion of mSin1 did not lead to appreciable differences in the F-actin levels compared to wildtype polarized cells (mSin1 KO, **Figure S1E**), suggesting the kinase arm of mTORC2 may be dispensable for regulating F-actin levels.

To investigate the role of mTORC2 on the spatial dynamics of actin regulation, we next focused on the subcellular features of F-actin distribution in polarised cells after 5 minutes of chemoattractant stimulation (**Figure 2B**), visualized via maximum-intensity projections of 3D data stacks. Rictor KO cells showed broader range of F-actin in the front compared to WT and mSin1 KO cells (**Figure 2B**). We used linescan (5 μm line ROI) to measure F-actin levels orthogonal to the leading front (**Figure 2C**) and fitted the F-actin intensity profile to a Bi-Gaussian to estimate the effective width of the F-actin zone (Buys and De Clerk, 1972). While WT and mSin1KO cells have very similar widths of F-actin zone (fitted width ~ 2-2.5 μm), Rictor depletion led to a two-fold expansion of the width of the actin front (fitted width 5.4 μm).

Recent lattice light sheet imaging data have shown that neutrophils generate not only substrate-bound protrusions but also axial protrusions that extend away from the plane of substrate (Fritz-Laylin *et al.*, 2017; Pipathsouk *et al.*, 2021). To investigate whether Rictor/mTORC2 plays a role in constraining the formation and abundance of these axial protrusions, we analyzed the extent of protrusion formation in 3D reconstructions of neutrophils. We used ChimeraX (Pettersen *et al.*, 2021) to 3D reconstruct and render these cells in two axial planes *yz* and *tilted xz* (**Figure 2D ii, iii, Video 1**). Confirming our expectation, loss of Rictor led to enhanced accumulation of F-actin rich protrusions away from the plane of the substrate. These protrusions were frequently present (> 50 % of all cells imaged; **Figure 2E, Video 1**) in Rictor KO cells, and they were more rarely observed in WT or mSin1 KO cells (~ 25% of all cells; **Figure 2E**).

The absence of discernible defects in F-actin distribution in absence of mSin1 (and hence mTORC2 kinase activity) suggest that mTORC2 relies on its Rictor-dependent kinase independent signaling to restrict F-actin to the leading edge of cells (**Figure 2F**). Next, we investigated how mTORC2 regulates the biochemical effectors of front/back polarity in cell motility.

Kinase-independent arm of Rictor/mTORC2 inhibits Rac activity

The migration phenotypes we observe for both kinase-dependent and kinase-independent arms of Rictor/mTORC2 could arise from its engagement with different portions of the migration cascade (**Figure 3A**). A wide range of motile cells including neutrophils show a distinct front-back polarity and organise their protrusive fronts and contractile backs using Rac and RhoA/myosin signaling, respectively (Xu *et al.*, 2003). We were interested in how

mTORC2 regulates these polarity and cytoskeletal programs. Cellular stretch has been shown to inhibit Rac activity in several contexts (Katsumi *et al.*, 2002; Houk *et al.*, 2012), but it is not clear which arm of mTORC2 activities are necessary for this inhibition in neutrophils.

Here, we probed whether kinase activity of mTORC2 is dispensable restricting Rac activation and actin polymerization (**Figure 3A**). To investigate mTORC2 regulation of Rac, we leveraged a quantitative immunofluorescence assay to probe Rac activity following the phosphorylation profile of Rac effector p21-activated kinase (Pak) upon chemoattractant stimulation (Itakura *et al.*, 2013; Graziano *et al.*, 2019). While chemoattractant (fMLP) addition is sufficient to trigger downstream signaling and polarisation of neutrophil-like cells in suspension and is often used to assay Rac activity biochemically, we chose to carry out these assays on cells adhered to fibronectin coated glass (Itakura *et al.*, 2013). This approach enabled improved imaging for quantification and reliable comparison of the effects of mTORC2 perturbations using cells treated and plated in similar conditions (**Figure 3B-C** and **Figure S3C-D**). All cells (wildtype, Rictor KO, mSin1 KO and mTOR inhibited wildtype) were able to polarise and organise the Rac activity (pPAK) at the leading edge after 3 min of chemoattractant stimulation (**Figure 3B**). Rictor KO cells exhibited elevated levels (~20-25% above wildtype) of sustained Rac activity. In contrast, perturbation of mTORC2 kinase activity (in mSin1 KO cells or upon mTOR kinase inhibition with KU) did not significantly alter Rac activation. We independently verified these results with alternate KO clones of Rictor and mSin1 targeting other genomic regions (**Figure S3 A,B**) and found Rac activity elevated in the alternate Rictor KO clone but not mSin1 KO clone (**Figure S3C**). The marked differences in Rac activity observed upon interfering with the kinase-independent (Rictor KO) but not kinase-

dependent arms of mTORC2 (mSin1 KO or mTOR kinase inhibition) suggests that kinase-independent roles of Rictor/mTORC2 are responsible for limiting leading edge Rac signals.

mTORC2 kinase activity stimulates myosin contractility at the trailing edge

Next, we investigated whether perturbation of mTORC2 activity also affects polarity signaling at the trailing edge of the cell. Active RhoA and its associated RhoA-Kinase (ROCK) localize and phosphorylate myosin regulatory light chain (pMLC) to power contraction of the trailing edge (Wong *et al.*, 2006; Tsai *et al.*, 2019). Biochemical studies in neutrophils have shown that mTORC2 kinase effector PKC regulates RhoA and myosin activity in neutrophils (Liu *et al.*, 2010, 2014). If kinase roles of mTORC2 stimulate myosin contractility, we expect both Rictor KO and mSin1 KO cells to show reduced pMLC levels (**Figure 3A**). If the RhoA/myosin inhibition is secondary to an increase in the antagonistic Rac activation, we would expect larger effects for Rictor KO cells.

We used immunofluorescence (IF) against phospho-MLC to probe myosin contractility in dHL-60 neutrophils plated on glass and stimulated with chemoattractant (25 nM fMLP) for 5 minutes to allow cells to polarize (images, **Figure 3C**). We find all three conditions (Rictor KO, mSin1 KO and mTOR inhibition using KU) lead to profound loss of pMLC activation (~50-60% reduction, **Figure 3C**). We verified these results independently with alternate KO clones of Rictor and mSin1, which both showed similar reduction in pMLC levels (**Figure S3D**). Finally, we extended these analyses to primary human neutrophils where we can inhibit mTOR kinase activity with KU and assay pMLC level using similar assay condition and readouts as dHL-60 cells (**Figure 3D**). Experiments in primary human neutrophils confirmed that mTOR kinase

inhibition also leads to profound decrease (~40-50%) of pMLC upon chemoattractant stimulation.

In summary, our results show that the kinase-independent roles of Rictor/mTORC2 inhibit Rac activity in the front, while the kinase roles of mTORC2 stimulate contractility at the back, potentially enabling the two divergent downstream arms of mTORC2 to independently regulate the front and back polarity programs. We next explore the consequence of this regulatory circuit for front-back polarity coordination during motility.

Rictor/mTORC2 spatially and temporally coordinates the front and back polarity program during movement

Migrating neutrophils rely on front-back polarity coordination to persistently move, turn, and reorient during migration. This front-back coordination depends on multiple currencies including cell membrane tension (Houk *et al.*, 2012), actin flows (Maiuri *et al.*, 2015), myosin contractility (Tsai *et al.*, 2019), and biochemical signaling crosstalk (Xu *et al.*, 2003; Ku *et al.*, 2012) between the front and back polarity programs. Our results (**Figure 3**) suggest that neutrophils leverage the two arms of mTORC2 downstream signaling to coordinate front and back polarity signaling. We asked whether this logic contributes to the spatial organisation and temporal coordination of polarity during movement (**Figures 4, S4 and S5**).

To investigate the role of mTORC2 in front/back coordination, we revisited the agarose overlay conditions (Bell *et al.*, 2018; Brunetti *et al.*, 2022) that sensitized Rictor-dependent migratory phenotypes (**Figure 1E-G**). To map the distribution and coordination of polarity in migrating cells, we co-expressed localization biosensors for both active Rac (from Pak;

Srinivasan et al., 2003) and active RhoA (from Anilin; Piekny and Glotzer, 2008) in wildtype and Rictor KO cells and imaged them at high spatial and temporal resolution (frame interval of 3 second) in presence of uniform chemoattractant 25 nM fMLP (**Figure 4A, B montage, Video 2**). First, we assessed the spatial features of front and back regulation in these cells. Active Rac forms a gradient in front half of a polarised wildtype cell, while active RhoA is tightly focused at the rear (**Figure 4A**, WT). A linescan in the direction of cell movement (front-back axis) reveals the mutually exclusive distribution of biosensor and a strong anti-correlation (Pearson's R = 0.49 for WT; **Figure 4C**). While Rictor KO (**Figure 4B**) and mSin1 KO (**Figure S5A)** cells also polarise, they do so with an elongated stalk at the cell back (arising from low contractility), where the bulk of RhoA biosensor fluorescence is concentrated. However, wildtype and mSin1 KO cells showed strong mutual antagonism of Rac and RhoA, with RhoA activity completely excluded from the Rac-positive zones in the cell front (**Figure 4C and S5B**). In contrast, Rictor KO cells showed local hotspots of RhoA biosensor localisation in the cell front (**Figure 4D**). This impaired spatial sorting of front and back polarity signal can be detected by poor anti-correlation between both biosensors (Pearson's R = -0.22 for Rictor KO; **Figure 4D**). Front-back correlation (**Figure 4E**) quantified from several cells (WT = 23 cells; Rictor KO = 33 cells and mSin1 KO = 20 cells) shows significantly elevated correlation values thereby suggesting poorer front/back separation (Median for WT= - 0.55; Rictor KO = 0.1; mSin1 KO = -0.5). These defects originate specifically from differences in biosensor distribution across the front-back axis, as lateral linescan perpendicular to direction of movement (**Figure S4A, B and S5C**) do not show any preferential bias and resulted in similar overall distribution of Pearson correlation across the lateral plane for wildtype, Rictor KO and mSin1 KO cells (**Figure S4C**).

Next, we probed the temporal coordination of front-back polarity during movement under agarose. Recently, we used a polarity metric based on the centroid of biosensor intensity with respect to the geometric centroid of the cells to monitor Rac polarity (Graziano *et al.*, 2019). We revised this analysis approach to compute the centroid of biosensor intensities for both the Rac and RhoA biosensor (polarity vectors for WT and Rictor KO in **Figure 4A, B**). The distance between the zones of Rac and RhoA activation (inter-centroid distance) provides a measure of separation between front and back signals during migration (length between arrowheads of polarity vectors for WT and Rictor KO in **Figure 4A, B**). Cells proficient in coordinating front-back polarity during persistent movement exhibit smaller fluctuations in inter-centroid distance (Wildtype in **Figure 4F**). Rictor KO cells show enhanced amplitude of fluctuations for front/back separation (**Figure 4F**). We quantified the strength of these fluctuations as coefficient of variation (CV), a commonly used metric to quantify fluctuations in cell polarity (Lai *et al.*, 2018; Onwubiko *et al.*, 2019). Loss of Rictor leads to a stronger phenotype and significant increase in CV (**Figure 4G**; Median CV for WT: 0.2, Rictor KO: 0.5 and mSin1 KO: 0.35) while mSin1KO cells also exhibit a modest phenotype in front-back coordination. These results indicate that loss of Rictor can perturb both kinase-dependent and independent arms of mTORC2 which allow coordination between the polarity signals at front and back.

Our experiments probe how different branches downstream of mTORC2 activation (kinase dependent vs independent) relate to regulation of front-back polarity programs and their spatiotemporal coordination during movement. We next investigated whether biochemical signals and physical forces synergize to active mTORC2 in the first place.

Mechanical stretch synergizes with PIP$_3$ generation to activate mTORC2

TORC2 is an ancient program that has been shown to be regulated by both biochemical and mechanical inputs in several contexts ranging from yeasts to Dictyostelium to immune cells. While mechanical stretch is one important regulator of the activation of the complex in *Dictyostelium* mounting evidence suggest biochemical inputs from Ras(and Rap) are required for full activation of the complex (Artemenko *et al.*, 2016; Khanna *et al.*, 2016). We have previously shown mechanical stretch can activate mTORC2 activity in neutrophils (Diz-Muñoz *et al.*, 2016). Here, we carry out a more systematic analysis of whether mechanics synergizes with biochemical inputs (as likely to happen in cells) to robustly amplify mTORC2 signaling outputs. To investigate whether mechanical stretch suffices to activate the mTORC2 complex, we exposed neutrophils to hypotonic media (50% decrease in ionic strength) and assayed the activation of mTORC2 via Akt phosphorylation. Hypotonic exposure (purely mechanical input) stimulates modest levels of mTORC2 activity, much less compared to purely chemoattractant stimulation (**Figure 5B, C**). Surprisingly, hypotonic exposure paired with chemoattractant addition (combination of biochemical and mechanical inputs) can robustly activate mTORC2 and amplify(~ 2 fold) its signaling output (**Figure 5B, C**). These results suggest that mechanical stretch from plasma membrane synergizes with other biochemical inputs from chemoattractant to amplify mTORC2 signaling activity.

Chemoattractant fMLP activates a wide range of downstream signaling pathways (G$\beta\gamma$, PI3K, Ras; Xu et al., 2003). Which of these programs are necessary to synergize with mechanical inputs to amplify mTORC2 outputs? Here we focused on the PI3K node that is responsible for PI-3,4,5-P$_3$ (PIP$_3$) generation at the front of the cells. PIP$_3$-Rac positive feedback is central for instructing actin polymerisation in the front and raising cellular tension

(Wang *et al.*, 2002; Weiner *et al.*, 2002). Moreover, PIP_3 is also responsible for recruitment of mTORC2 phospho-substrate Akt (Ebner *et al.*, 2017b, 2017a). In neutrophils, PI3Kγ is the dominant regulator of fMLP-dependent PIP_3 production (Stephens *et al.*, 1994; Hannigan *et al.*, 2002). To test if PI3Kγ activity is a necessary for stretch-dependent amplification of mTORC2 activity we used PIK90 (Van Keymeulen *et al.*, 2006), a specific inhibitor of PI3Kγ (**Figure 5D**). dHL-60 cells pre-treated with PIK90 and subsequently stimulated with fMLP alone or in combination with hypotonic media (50% osmolarity) show background (basal) levels of pAkt in immunoblots compared to untreated cells (**Figure 5E, F**). These results show that PI3Kγ induced PIP_3 synthesis is necessary for neutrophils to activate and amplify mTORC2 kinase activity upon osmotic stretch.

Finally, we tested whether PIP_3 is sufficient to replace chemoattractant in mechanics-synergized mTORC2 activation. For this purpose, we used an optogenetic module (opto-PI3K) which can synthesize PIP_3 in response to light stimulation (Graziano *et al.*, 2017) (**Figure 5G**). Optogenetic stimulation of PIP_3 sufficed as the co-input with mechanical stretch in mTORC2 activation (**Figure 5H, I**). Our results indicate that PIP_3 and mechanical stretch jointly drive robust amplification of mTORC2 activity.

DISCUSSION

For persistent motility, neutrophils must coordinate the activation of their leading and trailing cytoskeletal networks (Houk *et al.*, 2012; Tsai *et al.*, 2019). The mTORC2 complex is a critical regulator of this coordination. Following protrusion-induced membrane stretch, mTORC2/Rictor activation inhibits actin polymerization to enable a dominant front to emerge (Diz-Muñoz *et al.*, 2016) and regulates myosin contractility at the trailing edge (Liu *et al.*,

2010). Here we use a combination of genetic nulls and pharmacological tools to investigate the kinase dependent and independent links from mTORC2 to these cytoskeletal programs. mTORC2 is indispensable for movement when neutrophil-like dHL-60 cells are mildly confined (~5 μm) under agarose to mimic the confined spaces these cells explore *in vivo* (**Figure 1**). The kinase-independent roles of Rictor/mTORC2 are central to regulating the leading edge polarity program (Rac activity, F-actin distribution; **Figures 2 & 3**) while its kinase activity stimulates myosin contractility at the trailing edge. Using dual biosensor imaging of front and back polarity program, we show that mTORC2 is necessary for the spatial and temporal coordination of polarity during movement (**Figure 4**). Finally, we probe the requirements for mTORC2 activation. Membrane-stretch synergized with the biochemical input PIP_3 to amplify mTORC2 activity (**Figure 5**). In summary, our results highlight the logic of stretch-activated Rictor/mTORC2 signaling in coordinating front-back polarity during neutrophil movement (working model in **Figure 6**).

TORC2 is an ancient regulator of plasma membrane (PM) tension homeostasis across evolution (Eltschinger and Loewith, 2016; Riggi *et al.*, 2020). In yeasts, an increase in PM tension triggers TORC2-based homeostatic responses to increase the surface area of the plasma membrane (Berchtold *et al.*, 2012; Riggi *et al.*, 2018). In Dictyostelium, the TORC2 signaling program is activated by shear stress and regulates polarity, chemotaxis and electrotaxis (Lee *et al.*, 2005; Kamimura *et al.*, 2008). In neutrophils, disruption of mechanosensory mTORC2 leads to elevated levels of membrane tension arising from increased actin polymerisation (Diz-Muñoz *et al.*, 2016). Among other immune cells, loss of Rictor in B-cells dramatically increases cortical F-actin levels following B-cell receptor (BCR) stimulation (Huang *et al.*, 2017). Similar mechanisms could also restrict actin polymerisation at

the tip of the leading edge of oligodendrocytes as they wrap around the axonal shaft during myelin sheath formation (Bercury and Macklin, 2015; Nawaz *et al.*, 2015), as mTORC2 signaling has been shown to regulate the differentiation, shape, and actin cytoskeleton organisation of these cells (Bercury *et al.*, 2014).

How does mTORC2 interface with cell polarity? While the kinase-independent roles of Rictor/mTORC2 inhibits the front (Rac); its kinase activity stimulates the back (RhoA). Using two distinct aspects of mTORC2 potentially enables independent regulation of the spatially polarised front and back program. Further, the use of a shared signalling node of mTORC2 activation may help facilitate coordination between the two polarity programs (**Figure 6**). This mTORC2-based mechanism of signaling based coordination between the two programs is likely to operate in conjunction with the recently reported fast mechanical coupling of protrusion and retraction dynamics observed in both neutrophils (Tsai *et al.*, 2019) as well as other cells that undergo ameboid migration (Liu *et al.*, 2015; Maiuri *et al.*, 2015).

How are downstream arms of Rictor/mTORC2 linked to regulation of front/back polarity signals? We show that the kinase independent arm of Rictor/mTORC2 inhibits Rac activation and actin polymerization at the leading edge (**Figures 2, 3**) consistent with some (Diz-Muñoz *et al.*, 2016) but not all (He *et al.*, 2013) previous studies, possibly owing to differences between the use of mTORC2 subunit knockdowns in previous work and complete knockouts in the present work. There are a number of potential mechanistic links from Rictor/mTORC2 to Rac activation. mTORC2 has been shown to directly interact with Rac1 (Saci *et al.*, 2011) and regulate Rac GEFs P-Rex1 and Tiam1 (Hernández-Negrete *et al.*, 2007; Morrison Joly *et al.*, 2017). Some of the kinase independent roles of mTORC2 could also arise from the scaffolding roles of Rictor independent of mTORC2 (Agarwal *et al.*, 2013; Gkountakos *et al.*, 2018). For

instance, Rictor participates in mTOR independent scaffolding complex with the unconventional Myo1c in adipocytes to regulate membrane ruffing (Hagan *et al.*, 2008), whose hematopoietic isoform Myo1g is a key regulator of cellular surface topology and membrane tension in other immune cells (Gérard *et al.*, 2014).

We find the kinase activity of mTORC2 *positively* regulates myosin contractility and tail retraction (**Figures 3, 4**). Our results are not consistent with an earlier study in neutrophils that had linked mTORC2 dependent phosphorylation of PKCβII to cAMP based *inhibition* of RhoA/pMLC activity (Liu *et al.*, 2010, 2014). This discrepancy could arise from the partial knockdown of a single subunit (Rictor by shRNA) analysed in the previous study, while in this study we have analysed independent clonal knockout lines for two sub-units (Rictor and mSin1) as well as pharmacologically inhibited mTOR kinase activity in both HL-60 neutrophil-like cells and primary human neutrophils to verify the positive link from mTORC2 kinase activity to pMLC (**Figure 3, Figure S3**) . Our results are consistent with earlier studies in Dictyostelium, where both Pia (Rictor) null and Rip3 (Sin1) null showed marked reduction in chemoattractant induced myosin assembly (Lee *et al.*, 2005). Moreover, the mTORC2 phospho-substrate PKC has been shown to increase myosin II contractility in neuronal growth cones (Yang *et al.*, 2013). Future work will identify the molecular players that act downstream of mTORC2 to regulate front-back polarity signals.

mTORC2 activation integrates several upstream inputs like chemoattractant, growth factors, Ras, and mechanical forces (Diz-Muñoz *et al.*, 2016; Khanna *et al.*, 2016; Kovalski *et al.*, 2019). In Dictyostelium, TORC2 activation relies on inputs from other leading edge components including Ras and Rap GTPase (Khanna *et al.*, 2016; Senoo *et al.*, 2019). We find that osmotic stretch can significantly amplify the signaling output of chemoattractant-

stimulated kinase activity of mTORC2. PI3K activity is necessary and sufficient for this amplification (**Figure 5**). Our results suggest that a combination of biochemical inputs and mechanical stretch can combine to trigger mTORC2 activity to inhibit actin assembly in protrusions that also contain the biochemical co-input PIP$_3$. PIP$_3$ could play this positive role by the joint recruitment of both the mTORC2 subunit mSin1 as well as the mTORC2 substrate Akt via their respective PH domains (Ebner *et al.*, 2017a, 2017b).

How might the activation of mTORC2 kinase activity be linked to its kinase-independent roles? Since mTORC2 activity is a mechanosensitive cascade (Berchtold *et al.*, 2012; Diz-Muñoz *et al.*, 2016), it is likely that the same sets of inputs we identify here (**Figure 5**) could trigger both mTORC2 kinase activity and its scaffolding roles either by recruitment of mTORC2 components (such as PIP$_3$/PH-domain interaction of mSin1 in mammalian cells; Ebner *et al.*, 2017a) or via local remodeling of mTORC2/Rictor scaffold interactors (such as the release of the TORC2 activator Slm1 from eisosomes in yeast; Berchtold *et al.*, 2012). There is a precedent for this in several other kinase with scaffolding roles including mTORC1 (Erbay and Chen, 2001; Rauch *et al.*, 2011). Similarly, the kinase activity of PI3Kγ and its kinase independent roles are both triggered downstream of β-adrenergic receptors and work in parallel to regulate cAMP levels (Patrucco *et al.*, 2004; Perino *et al.*, 2011).

A future challenge for the field will be to capture the spatial dynamics of the kinase-dependent and kinase-independent arms of mTORC2. An attractive hypothesis is that the kinase activity of mTORC2 could have a different spatial range to independently regulate myosin-based contractions in regions not constrained by PIP$_3$. Once mTORC2 kinase activity is triggered, it could induce the phosphorylation of myosin regulators that then diffuse to the trailing edge of the cell. There is a precedent for this in Dictyostelium where activation of

Akt/PKB at the leading edge controls a substrate PAKα that acts at the trailing edge (Chung *et al.*, 2001). Future imaging-based activity probes and will be necessary to address the spatial logic of mTORC2 activation during cell polarity and movement.

MATERIALS & METHODS

Cell Lines and culture

HL-60 cells were sourced from the laboratory of Henry Bourne and authenticated using short tandem repeat (STR) analysis. Cell culture was performed as described previously (Graziano *et al.*, 2019). HL-60 cells were cultured in RPMI-1640 with 25 mM HEPES and L-glutamine (Corning) with 10% (v/v) heat-inactivated FBS (Gibco) and 1X penicillin/streptomycin (Gibco) and maintained at 0.2–1.0 million cells/ml. HL-60 cells were differentiated with 1.5% DMSO (Sigma-Aldrich) at a starting density of 0.2 million/ml in growth media for 5 days to obtain neutrophil-like dHL-60 cells. All experiments were performed with dHL-60s unless otherwise stated. HEK-293T cells (to generate lentivirus for transducing HL-60s) were cultured in DMEM (Gibco) with 10% (v/v) heat-inactivated FBS. All cells were cultured in a 37°C/5% CO_2 incubator and routinely monitored for mycoplasma contamination every 6 months.

Plasmids

Plasmids were constructed using standard molecular biology protocols. DNA segments were PCR-amplified and cloned into a pHR lentiviral backbone and driven by promoter from spleen focus-forming virus (SFFV) via standard Gibson assembly between the MluI and NotI restriction sites. A construct for Rac biosensor PakPBD-mCherry was generated from

PakPBD-mCitrine (Graziano *et al.*, 2019) by switching the DNA encoding the fluorescent tag. The RhoA biosensor uses the AnillinAHPH domain (Piekny and Glotzer, 2008) and was obtained from Addgene (plasmid # 68026). The EGFP-AnilinAHPH was sub-cloned into pHR lentiviral backbone using similar sites and strategy as mentioned above. We modified our previously reported Opto-PI3K module from red-light sensitive Phy/PIF (Graziano *et al.*, 2017) to blue-light sensitive iLID (Guntas *et al.*, 2015). The Opto-PI3K module consists of two constructs which need to be co-expressed for exogenous PIP_3 generation - Construct A: iLiD-BFP-CAAX membrane anchor; Construct B: iSH2-EGFP-SspB scaffold for PI3-Kinase recruitment. Both constructs were assembled by Golden Gate-based cloning from a library of individual components from an extendable Mammalian Toolkit (Fonseca *et al.*, 2019) into the pHR vector backbone with EF1α promoter (for Construct A) or SFFV promoter (for Construct B). Guide RNAs (gRNAs) with homology to exon 2 of RICTOR (Rictor KO; 5' GTCCGCTGGATCTGACCCG 3'), exon 5 of Rictor (Rictor KO_2; 5' TAGCACCTTCTGGAGAATAC 3') ,exon 2 of MAPKAP1/mSin1 (mSin1 KO; 5' AGTCAGTCGATATTACCTCA 3') and exon 5 of MAPKAP1/mSin1 (mSin1 KO_2; 5' AAACAGTGACTTTAACTCCT 3') were selected using the CRISPR design tool in Benchling (https://benchling.com/) and cloned into the LentiGuide-Puro vector (Addgene plasmid #52963) as previously described (Sanjana *et al.*, 2014). The pHR vector used to express human codon–optimized *Streptococcus pyrogenes* Cas9-tagBFP was as previously described (Graziano *et al.*, 2017).

Lentiviral transduction of HL-60 cells

HEK-293Ts were plated in 6-well plates (Corning) and grown to 70–80% confluency. Cells were transfected with 1.5 μg of the pHR plasmid along with two plasmids containing the lentiviral packaging proteins (0.167 μg of pMD2.G and 1.3 μg of p8.91) with TransIT-293 (Mirus Bio). After 2–3 d of transfection, lentivirus-containing supernatant was collected, filtered with a 0.45-μm filter (EMD Millipore), and concentrated 40-fold with Lenti-X Concentrator (Takara). The concentrated lentivirus was used immediately or stored at −80°C. HL-60 cells were transduced by overnight incubation of 0.3 million cells with 4 μg/ml polybrene and ~130 μl of concentrated virus. Cells expressing desired transgenes were isolated by culturing in growth media supplemented with puromycin (1 μg/mL) or using fluorescence-activated cell sorting (FACS) as appropriate (FACS Aria3, BD Biosciences).

Generation of knockout cell lines using CRISPR/Cas9

RICTOR and MAPKAP1(mSin1) HL-60 KO cell lines were generated and validated as previously described (Graziano *et al.*, 2019). Wildtype HL-60 cells were transduced with a puromycin-selectable vector containing the gRNA sequence targeting the gene of interest. Following puromycin selection, cells were transduced with a *S. pyrogenes* Cas9 sequence fused to BFP. Cells expressing high levels of Cas9-BFP were isolated with FACS, after which a heterogeneous population was obtained and assessed by sequencing of the genomic DNA flanking the Cas9 cut site. Cells were then diluted into 96-well plates at a density of approximately one cell per well in 50% (vol/vol) filtered conditioned media from a healthy culture, 40% (vol/vol) fresh HL-60 media, and 10% (vol/vol) additional heat-inactivated FBS. Clonal cell lines were expanded and validated by genomic DNA sequencing to infer the indel distribution and immunoblots to assay loss of protein expression.

Preparation of human neutrophil

All blood specimens were obtained from healthy volunteers with informed consent and using minimal risk protocol approved by the Institutional Review Board at University of California San Francisco (Study 21-35147). Fresh samples of peripheral blood from healthy adult volunteers were collected via 23 gauge butterfly needles in 10 ml BD Vacutainer EDTA tubes (Becton Dickinson, New Jersey). Blood was kept on a shaker at minimum setting, and utilized within 2 hours of the draw. Neutrophils were isolated using the EasySep Direct Human Neutrophil Isolation Kit per the manufacturer's protocol (STEMCELL Technologies).

Cellular treatments and perturbations

Neutrophil-like dHL-60 cells were activated with chemoattractant formyl-Met-Leu-Phe (fMLP; Sigma) at effective final concentration of either 25 nM (for imaging based assays) or 100 nM (for cellular biochemistry). Acute increase in membrane tension and stretching was done by adding equal volume of hypotonic buffer (H_2O + 1 mM $MgCl_2$ + 1.2 mM $CaCl_2$) as described earlier (Houk *et al.*, 2012; Graziano *et al.*, 2019). mTOR kinase activity was inhibited by treating cells with 10 μM KU-0063794 (Selleckchem) for 30-45 mins in plain RPMI-1640. PI3Kinase activity was inhibited by incubating cells with 1 μM PIK-90 for 30-45 mins in plain RPMI as described earlier (Van Keymeulen *et al.*, 2006).

Cellular biochemistry

mTORC2 activity (phospho-Akt) assay

These assays were performed as described earlier (Graziano *et al.*, 2017). Cells (dHL-60; 5 days after differentiation) were serum starved to reduce basal pAkt signals by incubation in plain RPMI for 30-45 min at 37°C/5% CO_2 at a density of ~1.5 million cells/ml. All time courses were performed at room temperature around 25°C. For chemoattractant-based time courses (e.g., **Figure 5B**) cells were activated at final effective fMLP concentration of 100 nM, and samples were collected at indicated time points by mixing 0.5 ml of cells with 0.5 ml ice-cold stop solution (20% tricholoroacetic acid [TCA], 40 mM NaF, and 20 mM β-glycerophosphate). Samples were incubated at 4°C for at least 1h, after which proteins were pelleted, washed once with 0.75 ml ice-cold 0.5% TCA, and solubilized in 2x Laemmli sample buffer (Bio-Rad Laboratories). For pAkt assays (**S1 Figure C** and **Figure 5E**) cells were assayed in absence (basal level) or 3 minutes after 100 nM fMLP addition, as pAkt signals peaked at 3 min in our assays. Optogenetic stimulation of Opto-PI3K dHL-60 cells (**Figure 5H**) was done with the following modifications to the protocol above. Serum starved cells were placed in wells of a clear-plastic 24 well plate (Corning) and placed about 1 cm above a blue (450 nm) LED array. A ND4 filter (Sioti) was inserted between the cells and the LED light source to attenuate the illumination to 1mW. Cells were illuminated for 3 min following which the LED was switched off and chilled TCA was added to prepare samples as described above. Samples were then analysed by immunoblots. Quantification of these assays were done by calculating the ratio of band intensities of phospho-Pak (or Akt) to the total-Pak (or Akt). These values were then normalised to the peak values obtained for wildtype control in the time-series (fMLP 3 min for pAkt).

Immunoblot assay

Western blotting was done as previously described (Graziano *et al.*, 2017). Briefly, protein content from at least 0.75-1 million HL-60 cells was extracted by chilled TCA precipitation and resuspended in 2x Laemmli sample buffer. Protein samples were separated via SDS-PAGE, followed by transfer onto nitrocellulose membranes. Membranes were blocked for at least 1 hr in a 1:1 solution of TBS (20 mM Tris, 500 mM NaCl, pH 7.4) and Odyssey Blocking Buffer (LI-COR) followed by overnight incubation at 4 °C with primary antibodies diluted 1:1000 in a solution of 1:1 TBST (TBS + 0.2% w/v Tween 20) and Odyssey Blocking Buffer. Membranes were then washed 3x with TBST and incubated for 45 min at room temperature with secondary antibodies diluted 1:10,000 in 1:1 solution of Odyssey Blocking Buffer and TBST. Membranes were then washed 3x with TBST, 1x with TBS and imaged using an Odyssey Fc (LI-COR). Analysis was performed using Image Studio (LI-COR) and Excel. The following primary antibodies were used for the study; phospho-PAK1 (Ser199/204)/PAK2 (Ser192/197) (Cell Signaling #2605), PAK2 (3B5) (Cell Signaling #4825), phospho-Akt (Ser473; D9E) XP (Cell Signaling #4060), Akt (pan; 40D4; Cell Signaling #2920S), Rictor (Bethyl #A300-458A), mSin1 (Bethyl # A300-910A), and GAPDH Loading Control Antibody GA1R (Thermo Fisher). Secondary antibodies IRDye 680RD Goat anti-Mouse (LI-COR) and IRDye 800CW Goat anti-Rabbit (LI-COR) were used.

Transwell Assays

These assays were performed as previously described (Diz-Muñoz *et al.*, 2016). Briefly 0.3 million dHL-60 cells were stained with 5ul/ml DiD (Life Technologies) and plated on the upper chamber of the 24-well format HTS FluoBlokTM Multiwell Insert System (3 µm pore size; BD Falcon) in RPMI without phenol red (Life Technologies) with 2% FBS. Cells were allowed to

migrate towards the bottom well containing 20 nM fMLP for 1.5 hr at 37°C. The migrated cells were measured by fluorescence from the bottom of the insert using FlexStation 3 Microplate Reader (Molecular Devices). Migration index was calculated by dividing the amount of signal in the sample well by the signal in a well in which 0.3 million cells were plated in the bottom well. The dataset was normalised by the peak value obtained for wildtype cells (usually observed at 60 min).

Imaging Assays and Data Analysis

Microscopy hardware

We used a spinning-disk confocal microscope for all imaging data presented here. The setup comprised of a Nikon Eclipse Ti inverted microscope with following objectives (Plan Apo 10x/0.45 NA, 20x/0.75NA, 60x/1.40 NA, 100x/1.4 NA; Nikon), Yokogawa CSU-X1 spinning-disk confocal, Prime 95B cMOS camera (Photometrics), 4-line laser launch (405, 488, 561 and 640 nm laser lines; Vortran) and environmental control (37°C/5% CO_2; Okolab).

Preparation of cells for microscopy

Imaging based assays with dHL-60 cells were performed using 96-well #1.5 glass-bottom plates (Brooks Life Sciences). The wells were coated with a 100 µL solution of 10 µg/mL porcine fibronectin (prepared from whole blood) and 0.4 mg/mL bovine serum albumin (BSA, endotoxin-free, fatty acid free; A8806, Sigma) dissolved in Dulbecco's Phosphate Buffered Saline (DPBS; , Gibco) and incubated for 30 min at room temperature. Fibronectin solution was then aspirated, and each well was washed twice with DPBS. dHL-60 cells in growth media were pelleted at 300xg for 5 min, resuspended in 100 µL imaging media (RPMI1640 with 0.2 %

BSA), plated in each well and incubated (37°C/5% CO_2) for 20 minutes for cells to adhere. Primary human neutrophils were also plated as above and processed similarly as the dHL-60 cells for immunofluorescence assays.

F-actin staining

Cells were prepared and plated in 96-well glass bottom plate as described above and stimulated with 25 nM fMLP. After 5 minutes to allow cells to polarize, an equal volume of 2x fixation buffer (280 mM KCl, 2 mM MgCl2, 4 mM EGTA, 40 mM HEPES, 0.4% bovine serum albumin (BSA), 640 mM sucrose, 7.4% formaldehyde (w/v), pH 7.5) was added to each well and incubated for 15 mins at room temperature. The fixation buffer was then removed from each well and cells are washed once with intracellular buffer (140 mM KCl, 1 mM MgCl2, 2 mM EGTA, 20 mM HEPES, 0.2% BSA, pH 7.5). Following fixation, cells were treated with staining buffer (intracellular buffer + 0.2 % Triton X-100+ 5 μl/ml Alexa647-Phalloidin [Invitrogen]) for 30 mins in dark at room temperature. Cells were finally washed gently to remove excess staining buffer and 200 μl of intracellular buffer mixed with nuclear dye NucBlue (Thermofisher) was added to each well.

Immunofluorescence

Cells were prepared, plated, and fixed as above following which cells were incubated with permeabilization buffer (intracellular buffer and 0.2 % Triton X-100) for 20 mins at RT. Cells were then blocked (3% BSA and 1% normal goat serum in permeabilization buffer) for at least 1h at RT. Cells were incubated with primary antibody diluted in blocking solution for at least 2 hr at room temperature or overnight at 4°C. Cells were washed 3x with permeabilization buffer and then incubated with secondary antibody for 45 min-1h at room temperature. Finally, cells were washed 2x with permeabilization buffer and 1x with intracellular buffer before adding

fresh intracellular buffer mixed with NucBlue to each well for imaging. Phospho-PAK1 (Ser199/204)/PAK2 (Ser192/197) (Cell Signaling #2605) and phospho-Myosin Light Chain (Ser19) primary antibody (rabbit; Cell Signaling #3671) was used at 1:200 dilution with secondary antibody Goat anti-Rabbit IgG Alexa 488 (Invitrogen #A-11034) at 1:1000 dilution.

Image analysis for fixed preparations

All image analysis to measure the levels and distribution of F-actin and quantitative immunofluorescence (pPak or pMLC) was performed with Fiji/ImageJ. Briefly, raw images comprising z-stacks of several fields of cells obtained from the Nikon spinning disk confocal (ND2 format) were imported into Fiji. Before quantification, the image were background and flat field corrected using the background and flat-field fluorescence values estimated individually for all the different emission channels. Using the z-project tool in Fiji the corrected z-stacks were converted into maximum intensity projection for visualisation and sum-intensity projections for quantification of fluorescence. Intensity thresholds were estimated from the pixel intensity histogram to ignore background fluorescence pixels and uniformly applied to sum-intensity projections to identify cells, following which 'measure stack' function was used to measure intensity value for the whole field. Several fields (at least 20-50) with 10-15 cells each were pooled from multiple independent experiments to quantify the fluorescence levels of F-actin, pPak or pMLC (**Figures 2, 3, S1 and S3)** reported here and data was represented as box-plot to show the entire distribution of measured values. To quantify the width of the F-actin rich zone at cellular fronts (**Figure 2B, C)** , a 5 μm line ROI (2 μm wide;) was drawn from the front of the cell to obtain the intensity v/s length profile for each cell. Several cells (~20-30 for each condition) were measured and their respective profiles were averaged across the whole dataset. The averaged intensity profile was fitted to a Bi-gaussian distribution (Buys and De

Clerk, 1972) of skewed peak to account for the overall width of the F-actin rich zone. To visualize the 3D distribution of axial z-protrusions of cells, ROIs of individual cell z-stacks were imported into the 3D visualisation software UCSF-ChimeraX (Pettersen *et al.*, 2021) and intensity thresholded to highlight the F-actin structures and the cell nuclei. Fraction of cells with axial protrusions was calculated by visual inspection and counting of all cells with 3D-projections and the total number of cell nuclei in the entire field of F-actin stained cells.

Under-agarose preparation of HL-60s for imaging

Cells were prepared using standard under-agarose preparation techniques as described previously (Bell *et al.*, 2018; Brunetti *et al.*, 2022). Briefly, a solution of 2% w/v low melt agarose (Gold Bio) dissolved in RPMI1640 was prepared by heating the solution gently in a microwave. The solution was placed in a water bath at 37°C to cool down before adding to cells. In the meantime, dHL-60 cells were spun down at 300 x g for 3 mins and resuspended in plating media (RPMI + 2% FBS) at a concentration of 1 million/ml. 5 μl of cells were placed in the centre of a circular well (96 well plate; Greiner Bio-one) and allowed to settle for 5 min at RT. Agarose solution (195 μl) was then slowly dispensed into the well directly on the top of the cells. This allowed even deposition of agarose which congeals over 10-20 min at RT, following which the wells were monitored quickly under a standard tissue culture brightfield microscope and moved to the microscope to equilibrate at 37°C for another 20 mins prior to imaging.

Cell Motility Assays

Single cell motility assays were performed with cells plated in an under-agarose preparation (to mimic in-vivo like confined environment) or on fibronectin coated glass (standard unconfined 2D motility). For both types of motility assays, 0.1 million cells were labelled using 1μM CellTracker Green or Orange (Thermo Fisher) in plain RPMI for 10 min at 37C. Labelled cells

were spun down from labelling mix and washed once with plain RPMI and resuspended in imaging media (RPMI1640 + 0.5% FBS + NucBlue nuclear marker) and were either plated on fibronectin coated glass (as described above) or processed for under-agarose preparation and plates were moved to the microscope preheated to $37^{\circ}C$ for imaging. Cells were stimulated with a uniform concentration of 25 nm fMLP. To allow tracking of several cell nuclei, imaging was done using a low magnification objective (10x or 20x) to capture a larger field of view and imaged once every 30sec for over 20-30 min.Tracking of cell nuclei was performed using the Fiji plug-in TrackMate (Tinevez *et al.*, 2017). Cell nuclei tracks were filtered for desired property (duration of at least 10 min, high quality, not undergoing collisions) to obtain the coordinates of movement. Track features (like speed, persistence, displacement) were computed with inbuilt tools of Trackmate.

<u>Biosensor imaging</u>

To measure the extent of temporal coordination of front-back polarity, cells expressing both the Rac (PakPBD-mCherry) and RhoA (EGFP-Anilin-AHPH) biosensors were prepared and plated under agarose (2% w/v in RPMI1640) and stimulated with uniform chemoattractant (25 nM fMLP). Cells were imaged on spinning disk confocal at high spatial resolution (60X or 100X objective) with fast sequential acquisition (exposure time 100 ms) for 3 minutes at frame interval of 3 sec using a similar strategy as previously described (Tsai *et al.*, 2019). The raw images were background and flat-field corrected, and full images were manually cropped to a ROI with a single cell.

<u>Analysis for spatial distribution of polarity</u>

Spatial profiles of biosensor intensity were obtained from a line ROI (2 μm wide; 2 μm) starting at the leading edge and extending to the uropod to record the intensity v/s length traces for

both Rac and RhoA biosensor. Pearson's correlation coefficient between the two traces were computed for several such individual cells (at least 20-30, pooled from independent experiments) and plotted as box-plots. This metric provided an intuitive method to assess the front-back correlation (or lack of it in wildtype cells) of spatial distribution of polarity signals. To assess the lateral correlation, another line ROI was drawn near the centre of the same cells perpendicular to the front-back axis. Intensity profiles for both biosensors were recorded, and lateral correlation coefficients were calculated.

Analysis for temporal coordination of polarity

Cells which touch or collide with a neighboring cell were ignored from this analysis as they presented challenges to segmentation and further analysis. Single cells were then segmented by smoothing and intensity-based thresholding for each of the two emission channels for the biosensor intensities for every frame of the image sequence. The resulting binary images were then combined by taking the union of the two segmentations. Further analysis was done for sequence of frames where the segmented edge of the cell does not touch the boundary of the cropped image ROI. Using the consensus binary image described above, the weighted centroid of biosensor fluorescence intensity was calculated for each channel across frames. The distances between the coordinates of these centroids were calculated at each frame and the coefficient of variation (CV) of this series was calculated for each cell. CV provides a normalized metric for fluctuations in the inter-centroid distance over the course of the timeseries and can be readily compared for cells of varying sizes or across different genetic

background (say, wildtype or Rictor KO cells). The full analysis code is available on GitHub (https://github.com/orgs/weinerlab/repositories).

ACKNOWLEDGEMENTS

Author contributions: Conceptualization: S Saha, OD Weiner; Investigation and data curation: S Saha, JP Town; Formal Analysis: S Saha, JP Town; Reagents and Methodology: S Saha, JP Town; Funding acquisition : S Saha, JP Town, and OD Weiner; Software: JP Town; Visualization and Figures: S Saha, JP Town; Writing and revising: S Saha (original draft) with edits and inputs from OD Weiner and JP Town.

REFERENCES

Agarwal, NK, Chen, C-H, Cho, H, Boulbès, DR, Spooner, E, and Sarbassov, DD (2013). Rictor regulates cell migration by suppressing RhoGDI2. Oncogene 32, 2521–2526.

Artemenko, Y, Axiotakis, L, Borleis, J, Iglesias, PA, and Devreotes, PN (2016). Chemical and mechanical stimuli act on common signal transduction and cytoskeletal networks. Proc Natl Acad Sci U S A 113, E7500–E7509.

Bell, GRR, Natwick, DE, and Collins, SR (2018). Parallel High-Resolution Imaging of Leukocyte Chemotaxis Under Agarose with Rho-Family GTPase Biosensors. Humana Press, New York, NY, 71–85.

Berchtold, D, Piccolis, M, Chiaruttini, N, Riezman, I, Riezman, H, Roux, A, Walther, TC, and Loewith, R (2012). Plasma membrane stress induces relocalization of Slm proteins and activation of TORC2 to promote sphingolipid synthesis. Nat Cell Biol 14, 542–547.

Bercury, KK, Dai, JX, Sachs, HH, Ahrendsen, JT, Wood, TL, and Macklin, WB (2014). Conditional ablation of raptor or rictor has differential impact on oligodendrocyte differentiation and CNS myelination. J Neurosci 34, 4466–4480.

Bercury, KK, and Macklin, WB (2015). Dynamics and mechanisms of CNS myelination. Dev Cell 32, 447–458.

Brunetti, RM, Kockelkoren, G, Raghavan, P, Bell, GRR, Britain, D, Puri, N, Collins, SR, Leonetti, MD, Stamou, D, and Weiner, OD (2022). WASP integrates substrate topology and cell polarity to guide neutrophil migration. J Cell Biol 221.

Buys, TS, and De Clerk, K (1972). Bi-Gaussian fitting of skewed peaks. Anal Chem 44, 1273–1275.

Chung, CY, Potikyan, G, and Firtel, RA (2001). Control of Cell Polarity and Chemotaxis by Akt/PKB and PI3 Kinase through the Regulation of PAKa. Mol Cell 7, 937–947.

Diz-Muñoz, A, Fletcher, DA, and Weiner, OD (2013). Use the force: membrane tension as an organizer of cell shape and motility. Trends Cell Biol 23, 47–53.

Diz-Muñoz, A, Thurley, K, Chintamen, S, Altschuler, SJ, Wu, LF, Fletcher, DA, and Weiner, OD (2016). Membrane Tension Acts Through PLD2 and mTORC2 to Limit Actin Network Assembly During Neutrophil Migration. PLoS Biol 14, e1002474.

Ebner, M, Lučić, I, Leonard, TA, and Yudushkin, I (2017a). PI(3,4,5)P3 Engagement Restricts Akt Activity to Cellular Membranes. Mol Cell 65, 416-431.e6.

Ebner, M, Sinkovics, B, Szczygieł, M, Ribeiro, DW, and Yudushkin, I (2017b). Localization of mTORC2 activity inside cells. J Cell Biol 216, 343–353.

Eltschinger, S, and Loewith, R (2016). TOR Complexes and the Maintenance of Cellular Homeostasis.

Erbay, E, and Chen, J (2001). The mammalian target of rapamycin regulates C2C12 myogenesis via a kinase-independent mechanism. J Biol Chem 276, 36079–36082.

Fonseca, JP et al. (2019). A Toolkit for Rapid Modular Construction of Biological Circuits in Mammalian Cells. ACS Synth Biol 8, 2593–2606.

Frias, MA, Thoreen, CC, Jaffe, JD, Schroder, W, Sculley, T, Carr, SA, and Sabatini, DM (2006). mSin1 Is Necessary for Akt/PKB Phosphorylation, and Its Isoforms Define Three Distinct mTORC2s. Curr Biol 16, 1865–1870.

Fritz-Laylin, LK et al. (2017). Actin-Based protrusions of migrating neutrophils are intrinsically lamellar and facilitate direction changes. Elife 6, 1–41.

García-Martínez, JM, Moran, J, Clarke, RG, Gray, A, Cosulich, SC, Chresta, CM, and

Alessi, DR (2009). Ku-0063794 is a specific inhibitor of the mammalian target of rapamycin (mTOR). Biochem J 421.

Gérard, A, Patino-Lopez, G, Beemiller, P, Nambiar, R, Ben-Aissa, K, Liu, Y, Totah, FJJ, Tyska, MJJ, Shaw, S, and Krummel, MFF (2014). Detection of rare antigen-presenting cells through T cell-intrinsic meandering motility, mediated by Myo1g. Cell 158, 492–505.

Gkountakos, A, Pilotto, S, Mafficini, A, Vicentini, C, Simbolo, M, Milella, M, Tortora, G, Scarpa, A, Bria, E, and Corbo, V (2018). Unmasking the impact of Rictor in cancer: novel insights of mTORC2 complex. Carcinogenesis 39, 971–980.

Graziano, BR et al. (2019). Cell confinement reveals a branched-actin independent circuit for neutrophil polarity.

Graziano, BR, Gong, D, Anderson, KE, Pipathsouk, A, Goldberg, AR, and Weiner, OD (2017). A module for Rac temporal signal integration revealed with optogenetics. J Cell Biol 216, 2515–2531.

Guertin, DA, Stevens, DM, Thoreen, CC, Burds, AA, Kalaany, NY, Moffat, J, Brown, M, Fitzgerald, KJ, and Sabatini, DM (2006). Ablation in Mice of the mTORC Components raptor, rictor, or mLST8 Reveals that mTORC2 Is Required for Signaling to Akt-FOXO and PKCα, but Not S6K1. Dev Cell 11, 859–871.

Guntas, G, Hallett, RA, Zimmerman, SP, Williams, T, Yumerefendi, H, Bear, JE, and Kuhlman, B (2015). Engineering an improved light-induced dimer (iLID) for controlling the localization and activity of signaling proteins. Proc Natl Acad Sci 112, 112–117.

Hagan, GN, Lin, Y, Magnuson, MA, Avruch, J, and Czech, MP (2008). A Rictor-Myo1c complex participates in dynamic cortical actin events in 3T3-L1 adipocytes. Mol Cell Biol 28, 4215–4226.

Hannigan, M, Zhan, L, Li, Z, Ai, Y, Wu, D, and Huang, C-K (2002). Neutrophils lacking phosphoinositide 3-kinase γ show loss of directionality during N -formyl-Met-Leu-Phe-induced chemotaxis. Proc Natl Acad Sci 99, 3603–3608.

He, Y, Li, D, Cook, SL, Yoon, M-S, Kapoor, A, Rao, C V, Kenis, PJ a, Chen, J, and Wang, F (2013). Mammalian target of rapamycin and Rictor control neutrophil chemotaxis by regulating Rac/Cdc42 activity and the actin cytoskeleton. Mol Biol Cell 24, 3369–3380.

Hernández-Negrete, I, Carretero-Ortega, J, Rosenfeldt, H, Hernández-García, R, Calderón-Salinas, JV, Reyes-Cruz, G, Gutkind, JS, and Vázquez-Prado, J (2007). P-Rex1 links mammalian target of rapamycin signaling to Rac activation and cell migration. J Biol Chem 282, 23708–23715.

Hetmanski, JHR et al. (2019). Membrane Tension Orchestrates Rear Retraction in Matrix-Directed Cell Migration. Dev Cell 51, 460-475.e10.

Hind, LE, Vincent, WJB, and Huttenlocher, A (2016). Leading from the Back: The Role of the Uropod in Neutrophil Polarization and Migration. Dev Cell 38, 161–169.

Houk, AR, Jilkine, A, Mejean, CO, Boltyanskiy, R, Dufresne, ER, Angenent, SB, Altschuler, SJ, Wu, LF, and Weiner, OD (2012). Membrane tension maintains cell polarity by confining signals to the leading edge during neutrophil migration. Cell 148, 175–188.

Huang, L et al. (2017). Rictor positively regulates B cell receptor signaling by modulating actin reorganization via ezrin. PLoS Biol 15, 1–24.

Itakura, A, Aslan, JE, Kusanto, BT, Phillips, KG, Porter, JE, Newton, PK, Nan, X, Insall, RH, Chernoff, J, and McCarty, OJT (2013). p21-Activated Kinase (PAK) Regulates Cytoskeletal Reorganization and Directional Migration in Human Neutrophils. PLoS One 8, e73063.

Jacinto, E, Facchinetti, V, Liu, D, Soto, N, Wei, S, Jung, SY, Huang, Q, Qin, J, and Su, B (2006). SIN1/MIP1 Maintains rictor-mTOR Complex Integrity and Regulates Akt Phosphorylation and Substrate Specificity. Cell 127, 125–137.

Jacinto, E, Loewith, R, Schmidt, A, Lin, S, Rüegg, MA, Hall, A, and Hall, MN (2004). Mammalian TOR complex 2 controls the actin cytoskeleton and is rapamycin insensitive. Nat Cell Biol 6, 1122–1128.

Kamimura, Y, Xiong, Y, Iglesias, PA, Hoeller, O, Bolourani, P, and Devreotes, PN (2008). PIP3-Independent Activation of TorC2 and PKB at the Cell's Leading Edge Mediates Chemotaxis. Curr Biol 18, 1034–1043.

Katsumi, A, Milanini, J, Kiosses, WB, Del Pozo, MA, Kaunas, R, Chien, S, Hahn, KM, and Schwartz, MA (2002). Effects of cell tension on the small GTPase Rac. J Cell Biol 158, 153–164.

Van Keymeulen, A, Wong, K, Knight, ZA, Govaerts, C, Hahn, KM, Shokat, KM, and Bourne, HR (2006). To stabilize neutrophil polarity, PIP3 and Cdc42 augment RhoA activity at the back as well as signals at the front. J Cell Biol 174, 437–445.

Khanna, A et al. (2016). The small GTPases Ras and Rap1 bind to and control TORC2 activity. Sci Rep 6, 25823.

Koronakis, V, Hume, PJ, Humphreys, D, Liu, T, Horning, O, Jensen, ON, and McGhie, EJ (2011). WAVE regulatory complex activation by cooperating GTPases Arf and Rac1. Proc Natl Acad Sci 108, 14449–14454.

Kovalski, JR, Bhaduri, A, Zehnder, AM, Neela, PH, Che, Y, Wozniak, GG, and Khavari, PA (2019). The Functional Proximal Proteome of Oncogenic Ras Includes mTORC2. Mol Cell 73, 830-844.e12.

Ku, CJ, Wang, Y, Weiner, OD, Altschuler, SJ, and Wu, LF (2012). Network crosstalk dynamically changes during neutrophil polarization. Cell 149, 1073–1083.

Lai, H, Chiou, J-G, Zhurikhina, A, Zyla, TR, Tsygankov, D, and Lew, DJ (2018). Temporal regulation of morphogenetic events in Saccharomyces cerevisiae. Mol Biol Cell 29, 2069–2083.

Lämmermann, T, Afonso, P V., Angermann, BR, Wang, JM, Kastenmüller, W, Parent, CA, and Germain, RN (2013). Neutrophil swarms require LTB4 and integrins at sites of cell death in vivo. Nature 498, 371–375.

Lee, S, Comer, FI, Sasaki, A, McLeod, IX, Duong, Y, Okumura, K, Yates, JR, Parent, CA, and Firtel, RA (2005). TOR Complex 2 Integrates Cell Movement during Chemotaxis and Signal Relay in Dictyostelium. Mol Biol Cell 16, 4572–4583.

Liu, L, Das, S, Losert, W, and Parent, CA (2010). MTORC2 Regulates Neutrophil Chemotaxis in a cAMP- and RhoA-Dependent Fashion. Dev Cell 19, 845–857.

Liu, L, Gritz, D, and Parent, CA (2014). PKCβII acts downstream of chemoattractant receptors and mTORC2 to regulate cAMP production and myosin II activity in neutrophils. Mol Biol Cell 25, 1446–1457.

Liu, Y-J, Le Berre, M, Lautenschlaeger, F, Maiuri, P, Callan-Jones, A, Heuzé, M, Takaki, T, Voituriez, R, and Piel, M (2015). Confinement and low adhesion induce fast amoeboid migration of slow mesenchymal cells. Cell 160, 659–672.

Maiuri, P et al. (2015). Actin flows mediate a universal coupling between cell speed and cell persistence. Cell 161, 374–386.

Morrison Joly, M, Williams, MM, Hicks, DJ, Jones, B, Sanchez, V, Young, CD, Sarbassov, DD, Muller, WJ, Brantley-Sieders, D, and Cook, RS (2017). Two distinct mTORC2-

dependent pathways converge on Rac1 to drive breast cancer metastasis. Breast Cancer Res 19, 74.

Mueller, J et al. (2017). Load Adaptation of Lamellipodial Actin Networks. Cell 171, 188-200.e16.

Nawaz, S et al. (2015). Actin Filament Turnover Drives Leading Edge Growth during Myelin Sheath Formation in the Central Nervous System. Dev Cell 34, 139–151.

Onwubiko, UN, Mlynarczyk, PJ, Wei, B, Habiyaremye, J, Clack, A, Abel, SM, and Das, ME (2019). A Cdc42 GEF, Gef1, through endocytosis organizes F-BAR Cdc15 along the actomyosin ring and promotes concentric furrowing. J Cell Sci 132.

Patrucco, E et al. (2004). PI3Kgamma modulates the cardiac response to chronic pressure overload by distinct kinase-dependent and -independent effects. Cell 118, 375–387.

Perino, A et al. (2011). Integrating cardiac PIP3 and cAMP signaling through a PKA anchoring function of p110γ. Mol Cell 42, 84–95.

Pettersen, EF, Goddard, TD, Huang, CC, Meng, EC, Couch, GS, Croll, TI, Morris, JH, and Ferrin, TE (2021). UCSF ChimeraX: Structure visualization for researchers, educators, and developers. Protein Sci 30, 70–82.

Piekny, AJ, and Glotzer, M (2008). Anillin is a scaffold protein that links RhoA, actin, and myosin during cytokinesis. Curr Biol 18, 30–36.

Pipathsouk, A et al. (2021). The WAVE complex associates with sites of saddle membrane curvature. J Cell Biol 220.

Rauch, J, Volinsky, N, Romano, D, and Kolch, W (2011). The secret life of kinases: Functions beyond catalysis. Cell Commun Signal 9, 23.

Riggi, M et al. (2018). Decrease in plasma membrane tension triggers PtdIns(4,5)P $_2$

phase separation to inactivate TORC2. Nat Cell Biol 20, 1043–1051.

Riggi, M, Kusmider, B, and Loewith, R (2020). The flipside of the TOR coin - TORC2 and plasma membrane homeostasis at a glance. J Cell Sci 133.

Saci, A, Cantley, LC, and Carpenter, CL (2011). Rac1 Regulates the Activity of mTORC1 and mTORC2 and Controls Cellular Size. Mol Cell 42, 50–61.

Saha, S, Nagy, TL, and Weiner, OD (2018). Joining forces: crosstalk between biochemical signalling and physical forces orchestrates cellular polarity and dynamics. Philos Trans R Soc B Biol Sci 373, 20170145.

Sanjana, NE, Shalem, O, and Zhang, F (2014). Improved vectors and genome-wide libraries for CRISPR screening. Nat Methods 11, 783–784.

Sarbassov, DD, Ali, SM, Kim, D-H, Guertin, DA, Latek, RR, Erdjument-Bromage, H, Tempst, P, and Sabatini, DM (2004). Rictor, a Novel Binding Partner of mTOR, Defines a Rapamycin-Insensitive and Raptor-Independent Pathway that Regulates the Cytoskeleton. Curr Biol 14, 1296–1302.

Saxton, RA, and Sabatini, DM (2017). mTOR Signaling in Growth, Metabolism, and Disease. Cell 169, 361–371.

SenGupta, S, Parent, CA, and Bear, JE (2021). The principles of directed cell migration. Nat Rev Mol Cell Biol 22, 529–547.

Senoo, H, Kamimura, Y, Kimura, R, Nakajima, A, Sawai, S, Sesaki, H, and Iijima, M (2019). Phosphorylated Rho–GDP directly activates mTORC2 kinase towards AKT through dimerization with Ras–GTP to regulate cell migration. Nat Cell Biol 21, 867–878.

Srinivasan, S, Wang, F, Glavas, S, Ott, A, Hofmann, F, Aktories, K, Kalman, D, and Bourne, HR (2003). Rac and Cdc42 play distinct roles in regulating PI(3,4,5)P3 and polarity

during neutrophil chemotaxis. J Cell Biol 160, 375–385.

Stephens, L, Smrcka, A, Cooke, FT, Jackson, TR, Sternweis, PC, and Hawkins, PT (1994). A novel phosphoinositide 3 kinase activity in myeloid-derived cells is activated by G protein βγ subunits. Cell 77, 83–93.

Tinevez, J-Y, Perry, N, Schindelin, J, Hoopes, GM, Reynolds, GD, Laplantine, E, Bednarek, SY, Shorte, SL, and Eliceiri, KW (2017). TrackMate: An open and extensible platform for single-particle tracking. Methods 115, 80–90.

Tsai, TY-CYC et al. (2019). Efficient Front-Rear Coupling in Neutrophil Chemotaxis by Dynamic Myosin II Localization. Dev Cell 49, 189-205.e6.

Wang, F, Herzmark, P, Weiner, OD, Srinivasan, S, Servant, G, and Bourne, HR (2002). Lipid products of PI(3)Ks maintain persistent cell polarity and directed motility in neutrophils. Nat Cell Biol 4, 513–518.

Weiner, OD, Marganski, W a., Wu, LF, Altschuler, SJ, and Kirschner, MW (2007). An actin-based wave generator organizes cell motility. PLoS Biol 5, 2053–2063.

Weiner, OD, Neilsen, PO, Prestwich, GD, Kirschner, MW, Cantley, LC, and Bourne, HR (2002). A PtdInsP3- and Rho GTPase-mediated positive feedback loop regulates neutrophil polarity. Nat Cell Biol 4, 509–513.

Wong, K, Pertz, O, Hahn, K, and Bourne, H (2006). Neutrophil polarization: Spatiotemporal dynamics of RhoA activity support a self-organizing mechanism. Proc Natl Acad Sci 103, 3639–3644.

Xu, J, Wang, F, Van Keymeulen, A, Herzmark, P, Straight, A, Kelly, K, Takuwa, Y, Sugimoto, N, Mitchison, T, and Bourne, HR (2003). Divergent signals and cytoskeletal assemblies regulate self-organizing polarity in neutrophils. Cell 114, 201–214.

Yang, Q, Zhang, X-F, Van Goor, D, Dunn, AP, Hyland, C, Medeiros, N, and Forscher, P (2013). Protein kinase C activation decreases peripheral actin network density and increases central nonmuscle myosin II contractility in neuronal growth cones. Mol Biol Cell 24, 3097–3114.

Figure 1

A

Actin Protrusions

Membrane Stretch

Biochemical Signals

Front Polarity Signals

mTORC2 activity
Kinase Independent *Kinase Activity*

Back Polarity Signals Contractility

B

Subunit	Roles	Perturbation strategy	Expected Effects	
			Kinase activity	Kinase Independent
Rictor	Scaffolding; recruit substrates	CRISPR/Cas9 KO	X	X
mSIN1	Aids kinase activity	CRISPR/Cas9 KO	X	-
mTOR Kinase	Phosphorylates substrates	mTOR Inhibitor (KU)	X	-

C

WT Rictor KO
192_ Rictor
37_ GAPDH

WT mSin1 KO
75_ mSIN1
37_ GAPDH

D

Transwell migration (20 nM fMLP)

- Wildtype(n=6)
- RICTOR KO(n=3)
- mSIN1 KO(n=3)
- mTOR Inh (KU)(n=3)

Migration Index vs Time (min)

E

<5 µm

Under Agarose Motility (uniform 25 nM fMLP)

WT

Rictor KO

mSin1 KO

y-displacement (um)

x-displacement (um)

F

Mean Speed (µm/min)

p < 0.01   p < 0.01

WT   Rictor KO   mSin1 KO

G

Persistence (Disp. / Tot Dist.)

p < 0.01   ns

WT   Rictor KO   mSin1 KO

H

mTORC2 activity

Kinase independent   Kinase Activity

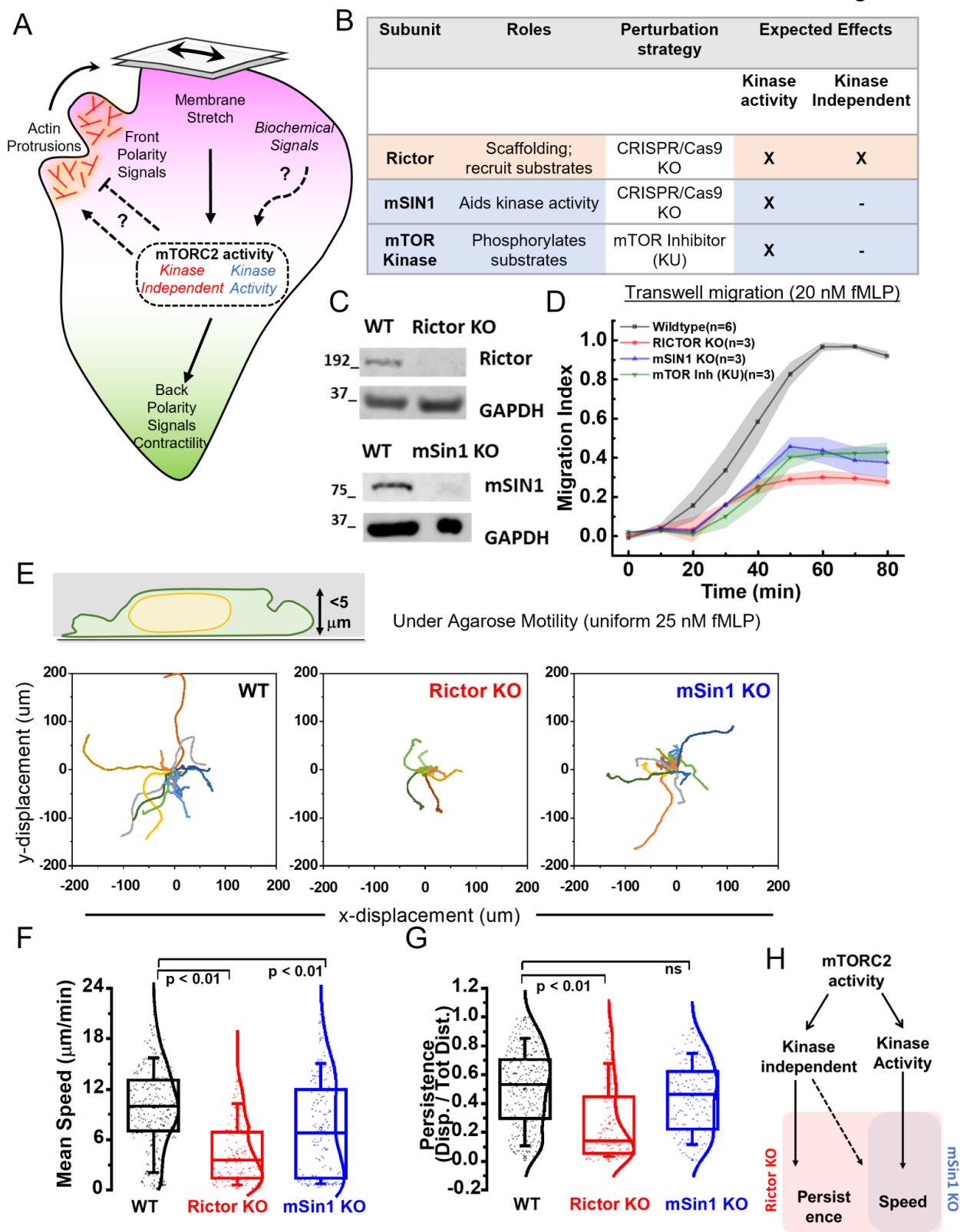Rictor KO

Persistence   Speed

mSin1 KO

Figure Captions

Figure 1. Rictor/mTORC2 is a regulator of neutrophil motility.

(A) mTORC2 connects membrane stretch to regulation of front (magenta) and back (green) polarity programs, but how mTORC2 is activated (purely mechanical or requires biochemical co-inputs) and what aspect of mTORC2 activation (kinase-dependent vs independent roles) regulates these polarity signals is not understood.

(B) To dissect the roles of kinase-dependent and kinase-independent roles of mTORC2, we generated individual CRISPR-Cas9 knockout lines of key components of the complex: Rictor (which scaffolds and aids structural integrity of the complex) or mSin1 (which primarily aids kinase activity). Additionally, we use mTOR Kinase inhibitors (here KU-0063794; KU) to phenocopy mSin1 KO defects.

(C) Representative immunoblots of wildtype (WT) HL-60 cells and gene-edited Rictor KO (top) and mSin1 KO (bottom) clonal HL-60 line to validate the loss of Rictor or mSin1 protein expression. GAPDH was used as a loading control.

(D) Perturbation of mTORC2 activities in Rictor KO (n=3; red), mSin1 KO(n=3; blue) and via mTOR Kinase inhibitor (KU; n=3; green) all led to defective transwell migration towards chemoattractant 20nM fMLP in comparison to WT cells (n=6; black). Mean ± SEM is plotted, n indicates independent replicates.

(E) Schematic shows neutrophil-like dHL60 cell moving under an agarose (2%) overlay with uniform chemoattractant (25 nM fMLP). Randomly chosen representative tracks (15 each) of wildtype (WT), Rictor KO, or mSin1 KO cells over a 12 min observation window; axes show x-y displacement in μm. Rictor KO cells migrate poorly and have markedly shorter displacements.

(F, G) Box plots (with kernel smooth distribution curve) show mean speed (F) and persistence (G; ratio of displacement/distance) of individual tracks. Both Rictor KO and mSin1 KO cells show a significant reduction ($p<0.01$; one-way ANOVA with Tukey-means comparison) in migration speed compared to Wildtype (WT). However, only Rictor KO show a significant decrease in the persistence ($p<0.01$; one-way ANOVA with Tukey-means comparison). N = 294 (WT), 138 (RictorKO) and 165 (mSin1 KO) tracks from individual cells pooled across 3 independent experiments. For box plots, median is indicated by the line, inter-quartile range (IQR) sets the box width and error bars indicate 10-90th percentile.

(H) Schematic highlights the phenotypes observed for mSin1 KO and Rictor KO cells. Kinase-dependent roles of mTORC2 appear to regulate speed whereas kinase-independent role regulates both persistence and speed.
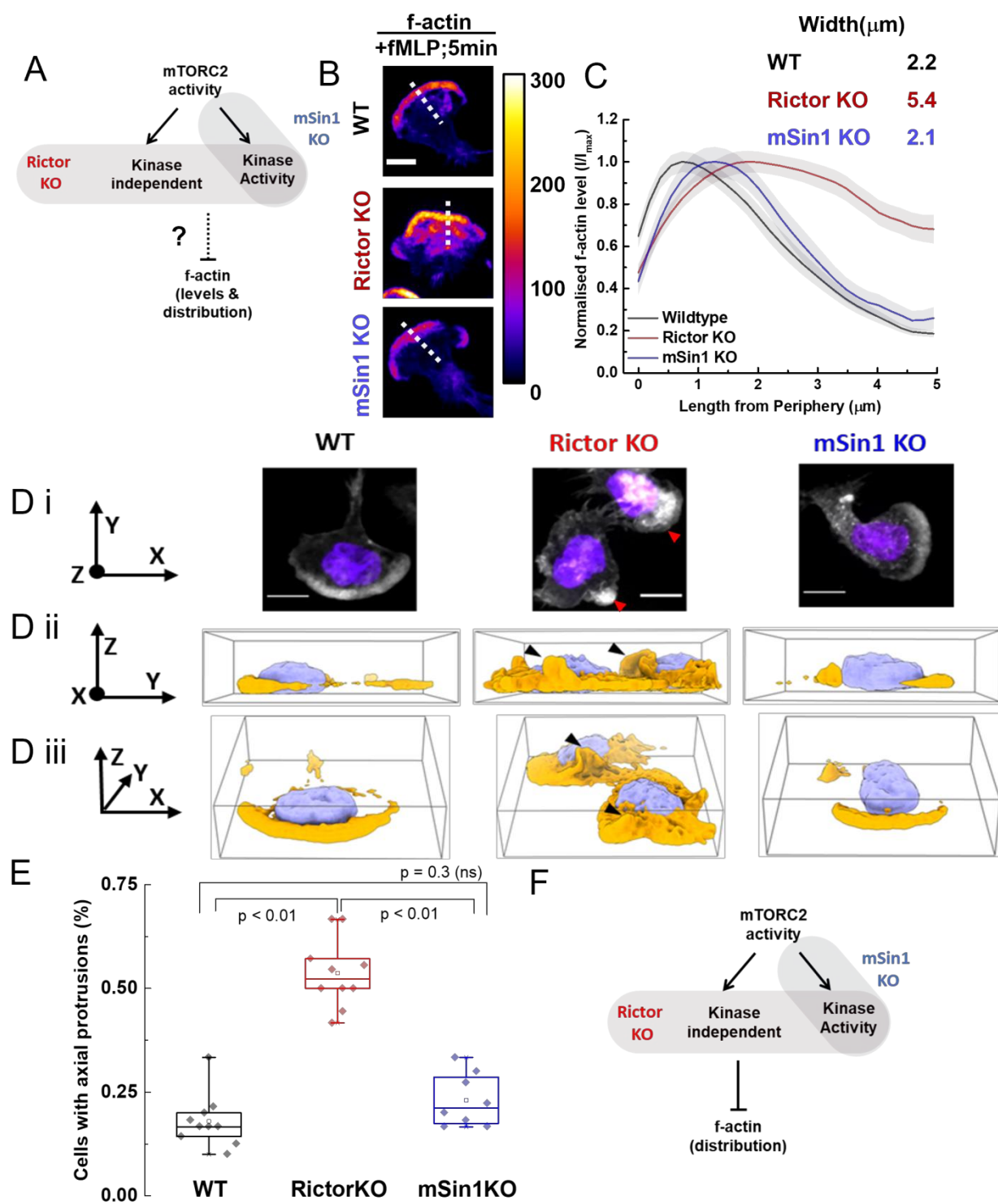
Figure 2

Figure 2. Kinase-independent arm of Rictor/mTORC2 restricts the zone of F-actin assembly to the front of the cells.

(A) Schematic shows how we are probing the kinase-dependent vs independent roles of mTORC2 in regulating F-actin levels and spatial organisation.

(B) Maximum intensity projections of Alexa647-phalloidin stained F-actin obtained from confocal z-stacks (10μm in z-depth) for wildtype (WT), Rictor KO, or mSin1 KO dHL60 cells, 5min after stimulation with 25nM fMLP. Fire-LUT shows the intensity scaling; scale bar 10 μm.

(C) F-actin intensity (normalized to individual peak) line-scans (Mean ± SEM) obtained (dashed lines on B) from wildtype (n=35), Rictor KO (n=48), or mSin1 KO (n=26) dHL60 cells pooled from two independent experiments. Rictor KO (red) has a wider lateral zone of leading edge F-actin in comparison to wildtype (WT; black) and mSin1 KO (blue); quantified by Bi-gaussian fitting of the intensity profile.

(D) Representative wildtype (WT), Rictor KO and mSin1 KO dHL60 cells shown as either maximum intensity projection (D i; *xy-plane*; scale bar 10 μm); or a ChimeraX 3D-reconstruction in *yz-plane* (D ii) and a tilted *xz-plane* (D iii) to highlight the axial features of F-actin (gold) distribution and nucleus (blue) as reference. Rictor KO cell shows protrusions out of the plane of the substrate that are rarely present in either Wildtype (WT) or mSin1 KO cells.

(E) Boxplots quantify fraction of cells with axial protrusions obtained from ChimeraX 3D-reconstructions views of each cell type (~10 fields; at least 100 cells analysed for each condition) across two independent experiments. RictorKO cells have significantly (p<0.01, one-way ANOVA with Tukey's mean comparison test) higher fraction of cells with axial protrusions. For box plots, median is indicated by the line, inter-quartile range sets the box width and error bars indicate 10-90th percentile.

(F) Defects observed in f-actin distribution for only RictorKO dHL60 cells but not mSin1 KO cells suggests kinase independent arm of Rictor/mTORC2 is required for negative feedback on f-actin assembly, distribution, and organisation.

Figure 3

A

Rictor KO

mTORC2 activity

mSin1 KO

Kinase independent arm

Kinase Activity

Front Polarity Rac Activity (pPAK)
?

?

Back Polarity Contractility (pMLC)

B

Rac activity (pPAK); 3 min post fMLP

Wildtype   Rictor KO   mSin1 KO   mTOR Inh.

Rac Activity (Norm. pPAK level)

p<0.05

p=0.6(ns)

p=0.2(ns)

Wildtype   Rictor KO   mSin1 KO   mTOR inhibitor

C

Myosin contractility (pMLC); 5 min post fMLP

Wildtype   Rictor KO   mSin1 KO   mTOR Inh.

Normalized pMLC level

p<0.001

p<0.001

p<0.001

Wildtype   Rictor KO   mSin1 KO   mTOR Inhibitor

D

Primary human neutrophil pMLC; 5 min post fMLP

Control   mTOR Inh.

Normalized pMLC level
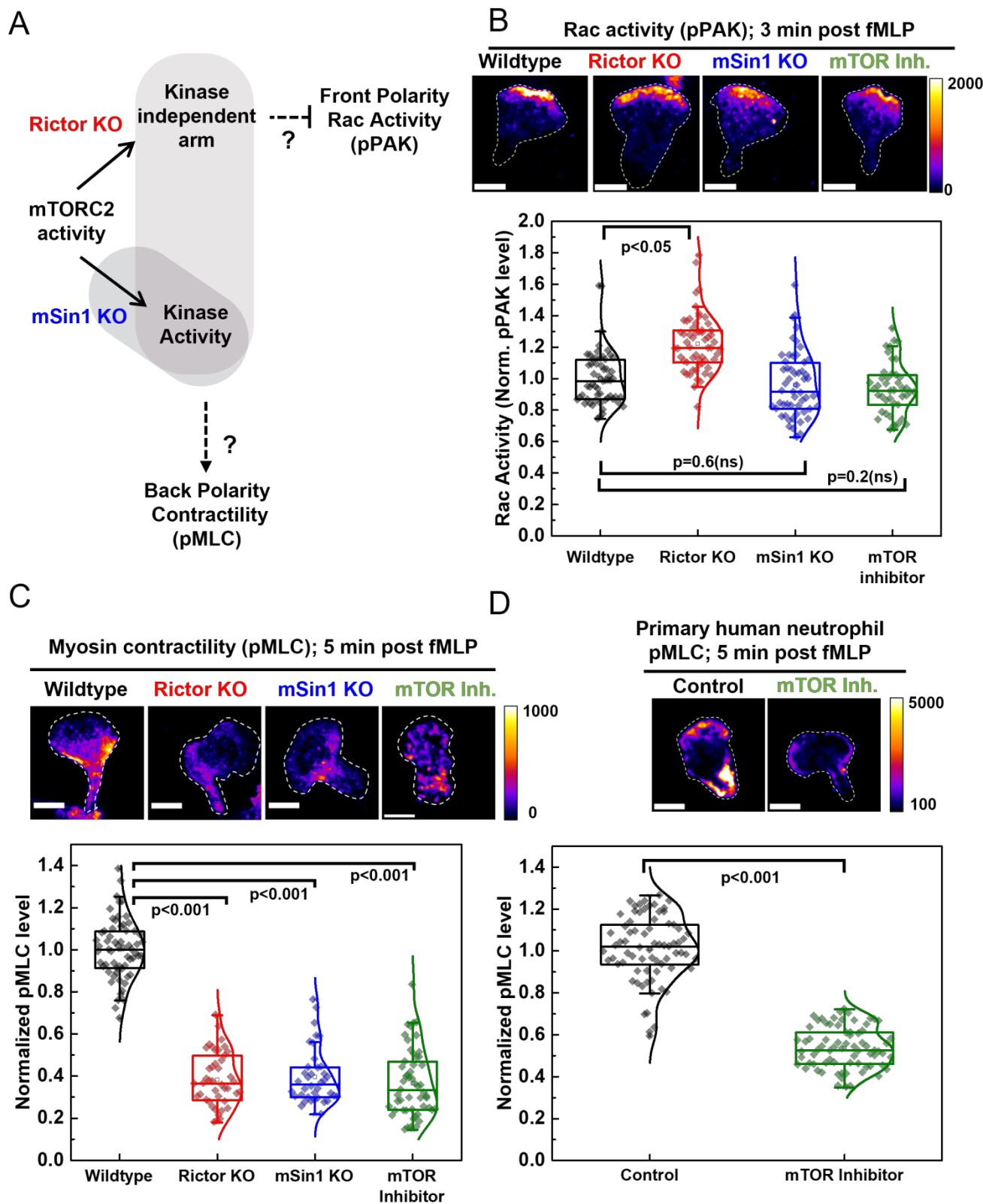
p<0.001

Control   mTOR Inhibitor

Figure 3. Kinase-independent arm of Rictor/mTORC2 inhibits Rac activity while its kinase role stimulates myosin contractility.

(A) Schematic shows how we probe the kinase-dependent vs independent roles of mTORC2 in regulating front (Rac activity) and back (myosin contractility) polarity programs.

(B) Phospho-PAK (pPAK) immunostaining (labelled with Alexa488 secondary antibody) of wildtype(WT), Rictor KO, mSin1 KO, and wildtype cells treated with mTOR Inhibitor (10 μM KU) adhered to fibronectin coated glass; 3 mins after stimulation with 25nM fMLP. Boxplots show the quantification of total pPAK intensity levels normalized to WT population from confocal z-stacks as shown above (40-50 fields and at least 300 cells for each condition) pooled from 4 independent experiments. Only Rictor KO cells exhibit significantly elevated pPAK levels compared to wildtype cells ($p<0.05$, one-way ANOVA with Tukey's mean comparison test).

(C) Phospho-myosin light chain (pMLC) immunostaining (labelled with Alexa488 secondary antibody) of wildtype(WT), Rictor KO ,mSin1 KO, and wildtype cells treated with mTOR Inhibitor (10 μM KU) adhered to fibronectin coated glass; 5 mins after stimulation with 25nM fMLP. Boxplots show the quantification of total pMLC intensity levels normalized to WT population from confocal z-stacks as shown above (30-50 fields and at least 300 cells across each condition) pooled from 3 independent experiments. Perturbation of mTORC2 kinase activity in Rictor KO, mSin1 KO and upon mTOR inhibition led to profound decrease in pMLC levels compared to wildtype cells ($p<0.001$, one-way ANOVA with Tukey's mean comparison test), suggesting that the kinase activity of Rictor/mTORC2 stimulates myosin contractility.

(D) Phospho-myosin light chain (pMLC) immunostaining of primary human neutrophils, either untreated (control) or mTOR inhibited (10 μM KU) adhered to fibronectin coated glass; 5 mins after stimulation with 25nM fMLP. Boxplots shows profound reduction total pMLC intensity levels in mTOR inhibited cells normalized to control population (~ 70 fields and at least 500 cells for both condition; $p<0.001$ by Mann-Whitney Test) pooled from 3 independent experiments and healthy volunteers.

All representative images (B-D) show maximum intensity projections obtained from 10 μm z-depth confocal z-stacks; scale bar 10 μm. Dashed outlines indicate the cell boundary, and all conditions were equally intensity scaled as shown by associated Fire LUT. For all box plots (B-D), median is indicated by the line, inter-quartile range sets the box width, and error bars indicate 10-90th percentile.

Figure 4

A Wildtype

B Rictor KO

Time (sec) | Image | Polarity Vectors

0:00, 0
0:18, 18
0:36, 36
0:54, 54
1:12, 72
1:30, 90

10 um

Active Rac (PakPBD-mCherry) Active RhoA (EGFP-Anilin AHPH)

Front-Back Spatial Profile

C
Rac Biosensor
RhoA Biosensor
Pearson's R: -0.49
Normalized Intensity (au)
Cell Length (Front - Back)

D
Rac Biosensor
RhoA Biosensor
Pearson's R: -0.22
Normalized Intensity (au)
Cell Length (Front - Back)

E
Front-Back Correlation
ns
p<0.01
p < 0.01
Wildtype   Rictor KO   mSin1 KO

F **Temporal Front-Back Coordination**
Wildtype
Rictor KO
Fluctuations in Inter-Centroid Distance (μm)
Time (sec)

G
p<0.01   p<0.05
p<0.05
Coefficient of Variation (CV)
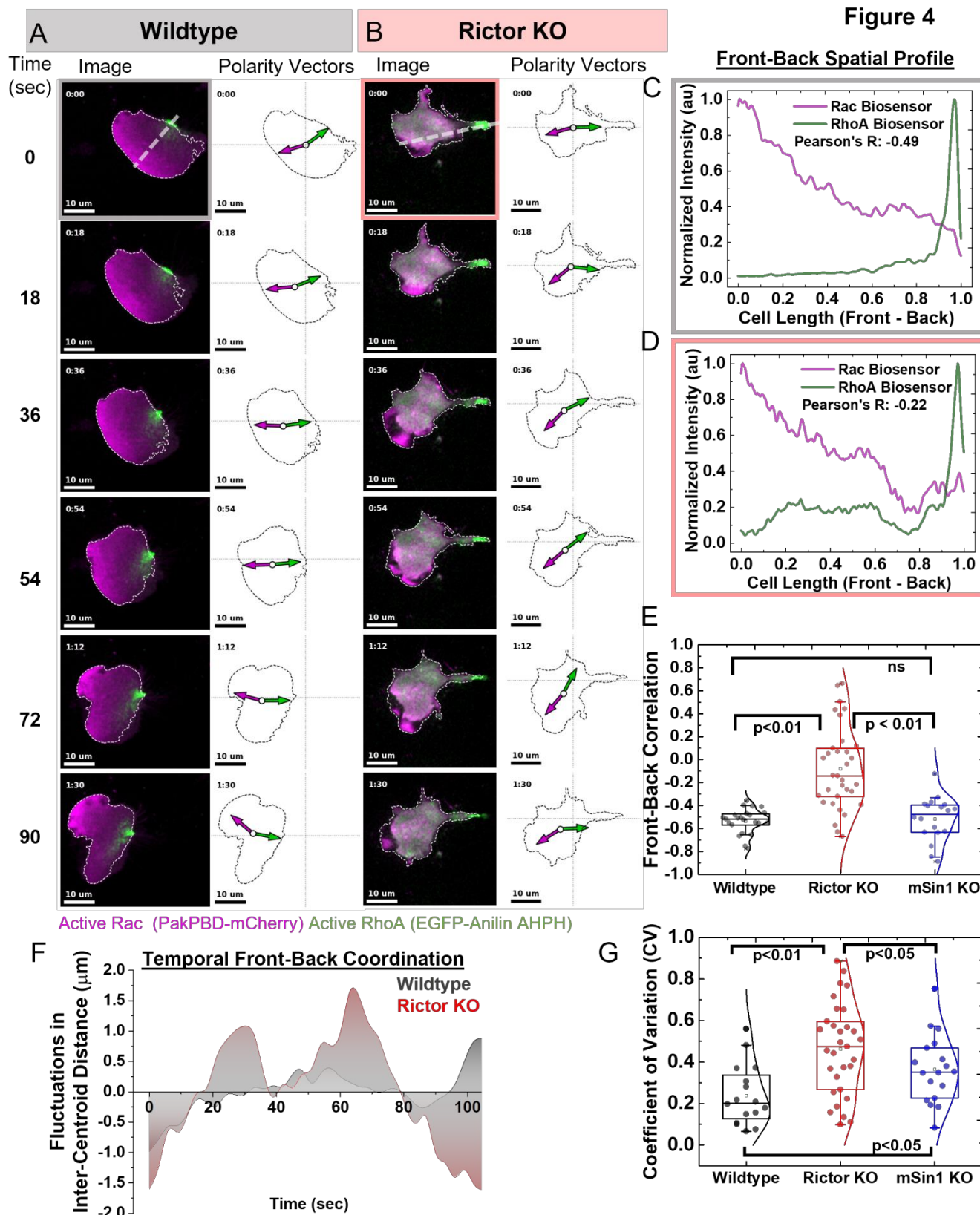Wildtype   Rictor KO   mSin1 KO

52

Figure 4. Rictor/mTORC2 is required for maintaining the spatial and temporal coordination of the front and back polarity programs.

(A) Wildtype (WT) and Rictor KO (B) cells co-expressing Rac biosensor (Pak-PBD-mCherry) and RhoA biosensor (EGFP-Anillin-AHPH) were plated under 2% agarose overlay and imaged every 3 seconds using a confocal spinning disk microscope. Montage of images acquired over 90 sec show the distribution of front (active Rac, magenta) and back (active RhoA, green) polarity signals (Image, left) and the corresponding front (magenta arrow) and back (green arrow) polarity vectors. The cell centroid for each frame is indicated by the open circle and it's displacement from the grid indicates overall cell movement; scale bar 10 μm.

(C, D) Anti-correlation between the intensity profile of polarity signals across the front-back axis provides a measure of spatial segregation of the front-back signals. Representative intensity profiles of Rac and RhoA biosensors obtained from line-scan (dashed line in time 0 sec in A, B) of wildtype (WT, C) and Rictor KO (D), with computed Pearson's correlation coefficient for each set of intensity traces (Pearson's correlation coefficient = - 0.49 for WT; - 0.22 for RictorKO). Lower Pearson's correlation coefficient indicates better separation between front and back signals.

(E) Boxplots of front-back correlation values for wildtype (WT, n=23 cells), Rictor KO cells (n= 33 cells) and mSin1 KO cells (n=20 cells) pooled from 4 independent experiments. Rictor KO cells have significantly higher correlation coefficient (p<0.01; one-way ANOVA with Tukey's mean comparison test) compared to both wildtype and mSin1 KO cells suggesting impaired spatial sorting of front-back polarity programs.

(F) To measure the extent of temporal coordination between polarity signals, we analyzed the fluctuations in the weighted inter-centroid distance between the front and back polarity biosensor intensities (indicated by the distance between the arrowheads of polarity vector in images A, B). Wildtype cells have polarity vectors uniformly aligned to the front-back axis and maintain a stable inter-centroid distance (gray), while RictorKO cells show stronger fluctuations in inter-centroid distance (red). Representative plot of fluctuations in inter-centroid distance for both cell types of WT and Rictor KO. We use coefficient of variation (CV) as a metric to quantify the magnitude of the fluctuations.

(G) Boxplots of distribution of CV obtained for wildtype(n =19 cells), RictorKO (n =30 cells) and mSin1 KO cells (n=16 cells) across four independent experiments. Rictor KO cells exhibit

significantly (p<0.01) higher fluctuations in ICD compared to both wildtype cells, while mSin1 KO cells also exhibit a modest yet statistically significant (p<0.05) phenotype. All statistical comparisons were done by one-way ANOVA with Tukey's mean comparison test. These results suggest impaired temporal coordination of front and back polarity programs in mTORC2 perturbed cells. For box plots, median is indicated by the line, inter-quartile range sets the box width, and error bars indicate 10-90th percentile.
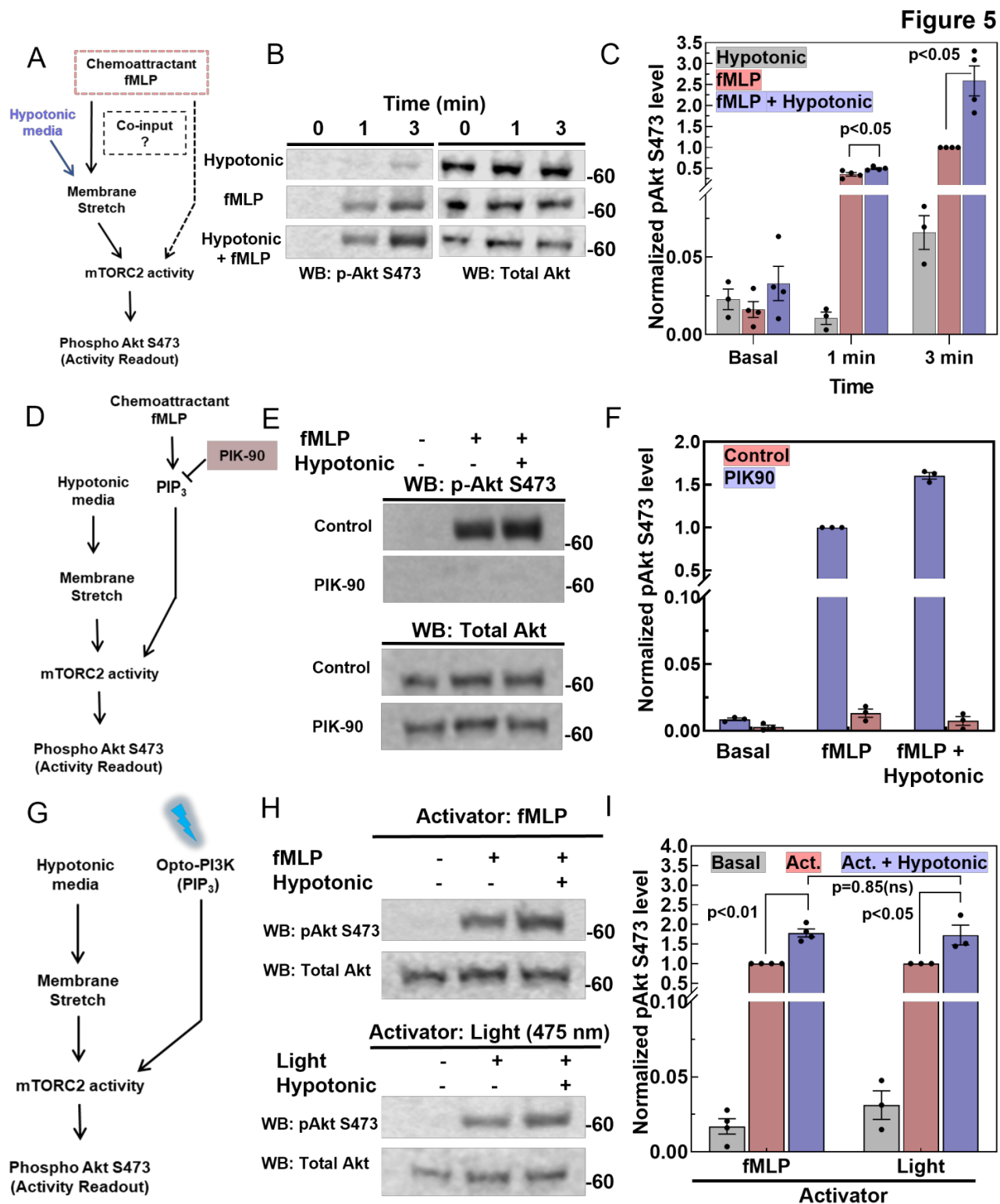
Figure 5. Mechanical stretch synergizes with PIP$_3$ generation to amplify mTORC2.

(A) Probing whether mTORC2 activation can be amplified by combination of mechanical stretch (here applied by 50% hypotonic shock) and additional biochemical inputs downstream of chemoattractant fMLP stimulation.

(B) To probe the logic of mTORC2 activity amplification, dHL-60 cells were subjected to either just hypotonic media (50% osmolarity reduction), stimulated with 100nM fMLP (fMLP only), or subjected to both inputs (hypotonic + 100 nM fMLP). mTORC2 activity was assayed in basal (0 min) and different time points (1 and 3 min) using phospho-Akt S473 and pan-Akt immunoblots, and representative immunoblot panels are shown.

(C) mTORC2 activity (pAkt/panAkt ratio) was quantified and normalized to 3min fMLP condition for each experiment; plotted as mean ± SEM from three independent experiments. Hypotonic shock (grey bars) alone stimulates very low levels of mTORC2 activity (gray bar), and chemoattractant addition is needed to trigger robust activation of signaling (red bar). However, a combination of fMLP and hypotonic shock (blue bar) significantly amplifies the signaling output of mTORC2 (p <0.05, unpaired t-test). Each bar represents mean ± SEM from three independent experiments.

(D) Probing the necessity of chemoattractant driven PIP_3 generation (using PI3Kγ inhibitor PIK-90) for synergistic amplification of mTORC2 activity upon hypotonic shock.

(E) Representative immunoblots of pAktS473 and pan-Akt to measure mTORC2 activation. Control (top) or PIK-90 (1μM; bottom) treated dHL60 cells were assayed for mTORC2 activity in absence (basal activity; -/- condition; left lane) or in presence of fMLP alone (+/-; middle lane) or a combination of fMLP and hypotonic shock (+/+; right lane). In presence of PIK-90, mTORC2 activity is severely attenuated (with background levels of pAkt S473 detected).

(F) mTORC2 activity (pAkt/panAkt) was quantified across the three conditions and normalized to control (fMLP alone) for each experiment; plotted as mean ± SEM from three independent experiments. The profound reduction of mTORC2 signaling output upon inhibition of PI3K activity suggests PIP_3 is a *necessary* co-input for activation (fMLP) and amplification of mTORC2 activity upon stretching (fMLP + hypotonic).

(G) Testing whether PIP_3 (via optogenetic activation) is sufficient to activate mTORC2 and can collaborate with mechanical stretch to amplify mTORC2 activation.

(H) Representative immunoblots of pAktS473 and pan-Akt of dHL60 cells activated either with chemoattractant (20 nM fMLP for 3 min; top panel) or using light at 475 nm (~1mW power for 3

min) to activate Opto-PI3K (bottom panel). For both inputs, pAkt/pan-Akt was assayed for basal (left lane; -/-), just stimulus (middle lane; +/-) or when paired with hypotonic media (right lane; +/+).

(I) mTORC2 activity (assayed by pAkt/AKT ratio) quantified across the three different conditions (H) for both activator (fMLP or light) and normalized using the activator only condition (just fMLP or light) for each experiment;plotted as mean ± SEM from three independent experiments. mTORC2 signaling activity is significantly boosted upon hypotonic shock (p<0.01 for fMLP; p <0.05 for Light; both by unpaired t-test) with similar extent of amplification observed when either fMLP or opto-PI3K was used as activator (p = 0.85, ns, unpaired t-test). This indicates PIP_3 generation is *sufficient* to synergize with mechanical stretch to amplify mTORC2 activity.
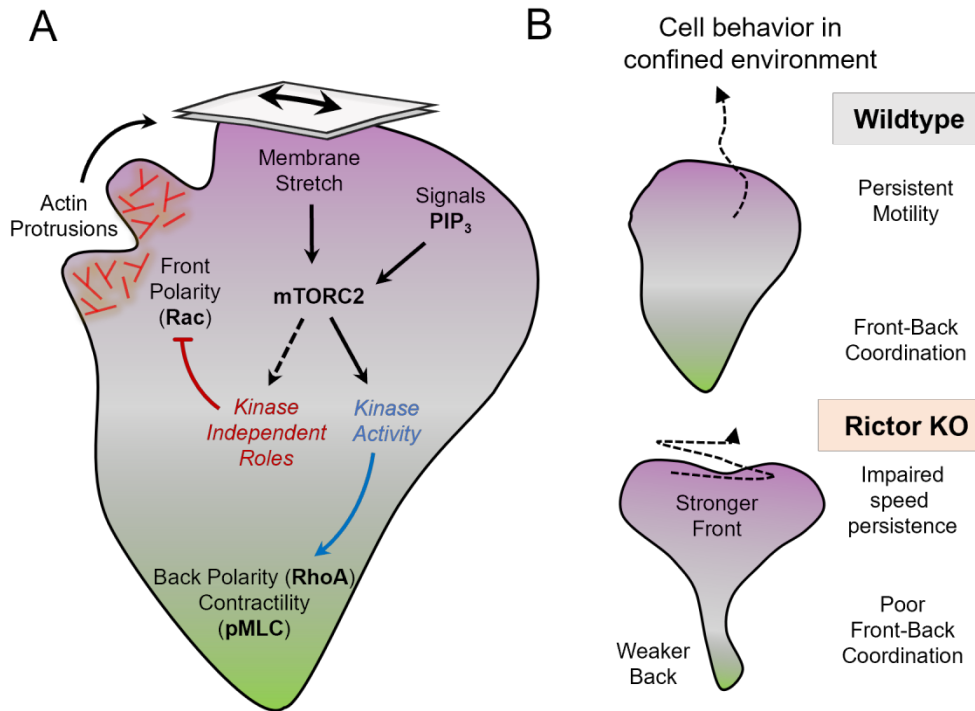
Figure 6

Figure 6. Working model for the molecular logic of mTORC2 based regulation of front and back cytoskeletal programs

(A) Membrane stretches and biochemical signals from PIP3 synergize to activate mTORC2 signaling programs and drive robust amplification of its kinase activity output. Noncatalytic kinase independent roles of Rictor/mTORC2 (black dashed arrow) allow stretch-dependent inhibition of front polarity signals (Rac) and restrict F-actin protrusion to the leading edge. The kinase roles of mTORC2 are necessary to stimulate myosin contractility (pMLC) at the back. While the spatial logic and molecular details of this circuit remains poorly understood, our results suggest this bifurcation of the downstream mTORC2 activities enables independent regulation of the spatially polarised front (magenta) and back (green) programs.

(B) The regulatory circuit for mTORC2 based front-back coordination (A) is essential for persistent movement in confined environments where cells experience mechanical stretch (like under agarose). In absence of mTORC2 activities (as in Rictor KO) cells exhibit elevated Rac activity (Stronger Front) and lowered contractility (Weaker Back); consequently front-back coordination is lost resulting in impaired speed and persistence of motility in confined environment.